WIND PRESSURES AND FORCES ON FLAT-PLATE PHOTOVOLTAIC SOLAR ARRAYS

by

N. Hosoya,* J. A. Peterka,** M. Poreh,***

and J. E. Cermak****

for

Boeing Engineering and Construction Company
P. O. Box 3707
Seattle, Washington 98124

Fluid Dynamics and Diffusion Laboratory
Civil Engineering Department
Colorado State University
Fort Collins, Colorado 80523

September 1980

*Graduate Research Assistant
**Associate Professor
***Professor
****Professor-in-Charge, Fluid Mechanics
and Wind Engineering Program

CER80-81NH-JAP-MP-JEC13

U18401 0075633

TABLE OF CONTENTS

LIST OF FIGURES

LIST OF FIGURES (Cont.)

LIST OF FIGURES (Cont.)

LIST OF TABLES

LIST OF TABLES (continued)

LIST OF SYMBOLS

Symbol	Definition
c	chord length of solar array
C_N	normal force coefficient
C_p	pressure coefficient
ΔC_{pmax}	maximum pressure difference
D	characteristic length in Reynolds number
FC	fence configuration
F(N)	velocity spectrum
H	ground clearance of solar array
H_{af}	height of additional fence
H_f	height of fence
H_s	height of spoiler
MC	model configuration
N	frequency
P	pressure
P_{af}	porosity of additional fence
P_f	porosity of spoiler
q_∞	dynamic pressure measured outside simulated boundary layer
q_{ref}	reference dynamic pressure
s	chordwise position--the edge where s = 0 corresponds to the leading edge for $\alpha \geq 90°$ and the trailing edge for $\alpha < 90°$
s_{max}	chordwise position where maximum pressure difference is observed
U	velocity of wind
U_{ref}	reference velocity of wind
U_{rms}	variance of fluctuating velocity

LIST OF SYMBOLS (Cont.)

Symbol	Definition
U_δ	velocity of wind at simulated boundary layer height
U_∞	velocity of wind measured outside simulated boundary layer
x	separation distance of solar array
x_f	seqaration distance between fence and solar array
α	angle of attack of solar array
δ	height of simulated boundary layer
ν	kinematic viscosity of air
ρ	density of air

1. INTRODUCTION

An important factor influencing the design and subsequently cost of large photovoltaic power generating systems, which involve a large number of simple structural elements and supports, is the magnitude of wind-induced loads. It has been recognized that usual design procedures, like the ANSI code (A58.1 - 1972) for example [1], are not adequate for accurate wind design of these repetitive, photovoltaic arrays with their distinctive configuration, orientation and limited height. In fact, the information presently available in the technical literature is not sufficient even for an optimum design of the structure for supporting a single photovoltaic array. Wind loads on individual arrays at different locations in a large array field are more difficult to determine as they vary according to the array location in the field and wind direction in a complicated manner. Higher loads are expected to exist at the edges of the field, but those can be reduced by carefully designed fences or barriers.

A theoretical study of the aerodynamics of flat plate arrays was recently made by Ronald D. Miller and Donald Zimmerman [2] at the Boeing Engineering and Construction Company (BECC). The study identified the basic features of the flat plate array loading which can be used for design purposes. It has been recognized by the authors, however, that theoretically derived design criteria are conservative and a wind-tunnel study of the wind loadings of such arrays was therefore recommended.

This report describes the experimental study of wind loading on flat plate photovoltaic arrays and array fields performed in the Meteorological Wind Tunnel of the Fluid Dynamics and Diffusion Laboratory at Colorado State University for BECC. The experimental program was developed in cooperation with Ronald D. Miller (BECC). The program's objectives were to determine the pressure distribution and forces acting on photovoltaic arrays for different angles of attack, two wind directions, head on winds and cornering winds (WD = 0° and 45° as defined in Figure 11) and two velocity profiles, as well as to investigate the effect of different fences and barriers on the wind loading at the edges and corners of an array field.

The wind-tunnel results were analyzed and the effect of the various parameters are presented in a form permitting calculation of the wind loading on prototype photovoltaic structures.

In view of the large number of data points collected in the report, it was found convenient to present most of the pressure measurements in a separate Appendix. The main report includes, however, a full description of the various runs and the calculated values of the normal force coefficient, the maximum local pressure coefficient and its location for each run in a tabulated form (Table 1 to 16) as well as a graphical representation of these data.

2. EXPERIMENTAL CONFIGURATION

2.1 Wind Tunnel

The Meteorological Wind Tunnel of the Fluid Dynamics and Diffusion Laboratory at Colorado State University (Figure 1) is characterized by a long (96 ft), slightly diverging test section, 6 ft-8 in. wide (at the turntable) and 6 ft high. The ceiling is adjustable to avoid pressure gradient along the test section. This facility is driven by a 400 HP variable pitch propeller with air flow velocity varying continuously from 0.5 fps up to 100 fps.

2.2 Flow Simulation

The primary consideration in modeling wind forces on structures in a wind tunnel is that the wind characteristics in the tunnel simulate natural boundary-layer winds at the actual site. In general this requires that the vertical distribution of mean velocity and turbulence in the wind tunnel boundary layer match those at the site and that the Reynolds numbers of the model and the prototype be equal. In addition, the small-scale model must be geometrically similar to its prototype. A detailed discussion of these requirements and their implementation in the wind-tunnel environment can be found in references 3, 4, and 5.

The construction of a 1:24 scale model of a prototype structure and its immediate surroundings (in this case, a flat, open area), submerged in a turbulent boundary layer of the Meteorological Wind Tunnel, shown in Figure 1, satisfies all the above criteria except those of equal Reynolds numbers and similarity of turbulence intensity and scale.

The kinematic viscosity ν appearing in the Reynolds number UD/ν is the same for both the tunnel and the full-scale structure. Because of this, the wind-tunnel air speed, U, would have to be 24 times the full-scale value if the model and prototype Reynolds numbers are to be equal. Testing at such high wind speeds is not feasible. However, for Reynolds numbers larger than 2×10^4 for sharp-edged structures where the flow separation point is fixed, there is no significant change in the values of aerodynamic coefficients as the Reynolds number increases. Since typical Reynolds number values are 10^6-10^7 for high-wind, full-scale flow and about 5×10^4 for wind-tunnel flows, acceptable flow similarity is achieved without equality of Reynolds numbers.

At a model scale of 1:24, the larger scales of turbulence in the atmospheric boundary layer are not simulated in the wind-tunnel flow. However, because the integral scale of the turbulence in the wind tunnel was 2 to 3 times the largest dimension of the model collector, the influence of the scale of turbulence is not expected to be significant [6]. Evidence exists which demonstrates some influence of turbulence intensity on drag of flat plates [6,7,8]. Because the turbulence intensity difference between the current simulation and a simulation with complete similarity of turbulent structure is not large, the effects due to turbulence intensity should be small. For cases where an upstream collector disturbs the approach flow, turbulence characteristics are dominated by the wake characteristics of the upstream object and possible differences due to turbulence intensity should further decrease.

An important factor which affects the wind loadings is the structure of the atmospheric boundary layer near the ground. The boundary layer which develops over a flat terrain is usually characterized by a non-uniform velocity profile which is closely described by a 1/7th power law mean velocity distribution. It is impossible to simulate in a wind tunnel the entire atmospheric boundary layer at the desired model scale for this study (1:24). One can, however, simulate the lower part of the atmospheric boundary layer in a 45 in. deep wind tunnel boundary layer [3-5].

The shape of the 1/7th power law boundary layer, which will be referred to as the Nonuniform flow 1 was obtained by means of selected roughness on the wind-tunnel floor upstream of the model. Forty ft of test section length were covered with 1 in. cubes followed by a 40 ft length of pegboard with 0.25 in. diameter pegs projecting 0.5 in. above the pegboard base (see Figure 2). In addition to the floor roughness, four triangular spires were installed at the test section entrance in order to get a thicker boundary layer than would otherwise be obtained. The normalized velocity and turbulence profiles of this boundary layer are shown in Figure 3 and data is tabulated in the Appendix. Turbulence intensity is the root-mean-square of the longitudinal fluctuating velocity divided by the local mean velocity. The turbulence intensity reached values of 20 percent in the boundary layer.

The spectrum of longitudinal velocity fluctuations is shown in Figures 4 and 5, including two suggested analytical models of velocity spectra for the atmosphere by Harris (9) and Davenport (10).

The spectra were obtained at 4 and 8 in. above the wind-tunnel floor. In this plot N is frequency, $F(N)$ is the velocity spectrum, U^2_{rms} is the variance of the fluctuating velocity, δ is the simulated boundary layer height (900 ft full-scale), and U_δ is the velocity at δ. The region where turbulence structure may be important to the determination of mean loading ranges upward from abscissa values of about 20 for wind speeds up to about 30 mph at 30 ft. Thus, the simulation has a turbulence intensity somewhat too high in the frequency range affecting mean wind loading on the model and too low in the low-frequency gusts.

The "Uniform Flow" velocity profile was obtained by placing the model at the upstream end of the test section. The measured velocity profile at that station, shown in Figure 6, indicates that a very thin boundary layer has developed along the short upstream section. Its effect on the wind loading on elevated panels is expected, however, to be small. A typical velocity distribution across the tunnel is shown in Figure 7.

2.3 The Models

Aluminum models of the flat photovoltaic array field having a geometrical scaling of 1:24 (Figure 2) and 1:12 (Figure 8) were constructed. (The 1:12 model was used in a limited number of tests only).

The chord size of the 1:24 model was $c = 4$ in., corresponding to a prototype value of 8 ft. Rows of pressure taps were drilled on each face of the array as shown in Figure 10. Each pressure tap represents the average pressure along a small section of the chord. The row at the edge of the array was used to study the wind loading at the side edge of the field.

To study the wind loadings on an array located in an array field, 1:24 scale models of array rows were constructed, which could be placed on the wind tunnel floor at desired locations to simulate the relative position in the field on the array with the pressure taps on which the wind loading was measured. Figure 2 shows a photograph of a 1:24 model of a photovoltaic array field in the wind tunnel. Figure 8 shows a photograph of the 1:12 model.

The fence was simulated in the model by perforated sheet metal, with holes of 3/16 in. diameter, having the same porosity (about 30 percent) as the prototype fence (see Figure 9).

3. INSTRUMENTATION AND DATA ACQUISITION

3.1 Measurements of Flow Characteristics

Velocity and turbulence intensity profiles for the approach flow under test conditions were made at the locations of the model in the tunnel (turntable) with the model removed.

The measurements were made with a Thermosystems Model 1050 constant-temperature anemometer with a 0.001 in. diameter platinum film sensing element 0.02 in. long. The sensing probe was attached to a vertical traverse to measure velocities and turbulent intensities at different heights. Output was processed through the Laboratory on-line digital data acquisition system.

Tests were made at only one wind speed in the tunnel around 50 ft/sec. This wind was sufficiently high to ensure Reynolds number similarity between the model and prototype.

The reference velocity at each test was measured using a pitot-static tube which was connected to a Setra differential pressure transducer. The pitot tube was placed outside the simulated boundary layer and recorded the value of $q_\infty = \rho U_\infty^2/2$, where ρ is the mass density of the air. The ratio of the reference velocity U_{ref}, at a prototype height of 10 m above the ground, to U_∞ was determined from the velocity distribution of the boundary layer according to the scale of the model. The value

$$q_{ref} = \frac{\rho U_{ref}^2}{2} = \frac{\rho U_\infty^2}{2} \left(\frac{U_{ref}}{U_\infty}\right)^2 \qquad (1)$$

at the height corresponding to 10 m above ground in the prototype was later used in calculating the dimensionless force and moment coefficients of the array, so that it was not necessary to measure the density of the air.

3.2 Pressure Measurements

Each pressure tap was connected through a pressure switch to a calibrated Setra differential transducer which measured the value of the local pressure above the ambient pressure at the test section away from the model. The output from the pressure transducers was recorded for 16 seconds at a 250 sample per second rate. The data was then analyzed by a Hewlett-Packard System 1000 minicomputer under program control and recorded. The minicomputer calculated the local pressure coefficients and using the reference total value q_{ref}, at 30 ft prototype height,

$$C_p = \frac{P}{q_{ref}} \tag{2}$$

3.3 Normal Force Calculations

The local force per unit area acting on each section of the array is equal to the difference in the pressures measured at the center of that section on the opposite faces of the array. The magnitude of this pressure difference is

$$\Delta p(s) = P(s)_{\text{lower face of array}} - P(s)_{\text{upper face of array}} \tag{3}$$

where s designates the position of the section as defined in Figure 11. A positive value of $\Delta p(s)$ will thus correspond to a

normal net force per unit area with an upward component as shown schematically in Figure 11.

The dimensionless local pressure difference is defined as

$$\Delta C_p = \frac{\Delta P}{q_{ref}} . \tag{4}$$

The maximum value of this coefficient, $\Delta C_{p_{max}}$ is of particular interest. The normal force N acting on the entire array can be calculated by integrating the value of $\Delta p(s)$ over the cord. Similarly, the normal force coefficient C_N is given by

$$C_N = \frac{N}{c} = \frac{1}{c} \int_o^c \Delta C_p(s)\, ds \tag{5}$$

The direction of a positive normal force is shown in Figure 11. In most cases one would expect to find negative values of C_N for $\alpha > 90°$.

4. PRESENTATION AND ANALYSIS OF THE EXPERIMENTAL DATA

4.1 Single Array Tests

Typical records of the pressure distribution on a single photovoltaic array for head-on winds (WD = 0°) in the uniform flow are shown in Figures 12-14.* The solid lines in Figure 12 show the local pressure coefficient distributions on the upstream face of the panel. Positive values are usually recorded on the upstream face. The pressure coefficients on the downstream face, marked by dashed lines, are negative and hardly vary across the panel, indicating a flow separation, which was observed in the flow visualization study for both the single array and many of the arrays in an array field, see for example Figure 31. The shape of the pressure distribution curves on the upstream face of the panel is almost symmetric for $\alpha = 90°$, but it becomes more and more skewed as the angle of attack decreases (Figure 12) or increases (Figure 13). Figure 14 shows the same data but for a large ground clearance, $H/c = \infty$ (actually measured at $H/c = 1.7$).

Comparing Figures 12 and 14 one finds that the pressure distribution on the upstream face of the panel is not affected to a large extent by the ground clearance. The back pressure, on the other hand, appears to change significantly. A value of $C_p \tilde{=} -1.35$ was recorded for $\alpha = 90°$, $H/c = \infty$, whereas a value of $C_p = -0.75$ was recorded for the same angle of attack with a ground clearance of $H/c = 0.25$. This reduction of the back pressure reduces significantly the normal force acting on the plate. Figure 15 shows the absolute values of

*Unless explicitly stated, the data refers to the measurements at the center of the array (see Figure 10).

the normal force for all the single array tests in a uniform flow. Evidently, the same effect is apparent at all angles of attack.

The reduced drag at small ground clearances may be due to the changes in the wakes caused by the reduction in the eddy size downstream of the panel. It should be recalled that the approach velocities in these tests are independent of height. The complicated nature of the interaction between these eddies and the flow, which determine the base pressure, makes it difficult to predict the value of these pressures theoretically.

The pressure distributions on a single array (H/c = 0.25) in a nonuniform flow are shown in Figures 16 and 17. A clear reduction of the pressure coefficients relative to those in the uniform flow is observed. The corresponding absolute values of the normal force for the two cases are shown in Figure 18. The average ratio $C_N(\text{uniform})/C_N(\text{nonuniform})$ is 1.43 $\pm$ 5% for these tests. This large reduction is primarily due to the relatively small wind speeds at the height of the array for the nonuniform velocity profile. It should be recalled that q_{ref} is measured at the height of 10 m above the ground whereas the center of the panel, for this value of ground clearance, varies from 3.36 ft for $\alpha = 20°$ to 6 ft for $\alpha = 90°$. The corresponding ratios of $q_{ref}/q_{\text{center of panel}}$ for these cases in a 1/7th power law velocity distribution are 1.89 and 1.61 respectively. Obviously, the difference in the dynamic pressure of the free stream at the height of the panel alone cannot fully explain the observed changes. Comparing the ratio of the back pressures in the two cases, for example, one finds an average ratio

of almost 2, whereas the ratio of the pressure coefficients on the upstream face of the panel is only around 1.5. The shape of the corresponding pressure distribution curves is also different for the two cases.

4.2 Array Field Tests

A wide field of photovoltaic arrays is characterized by the separation distance, x/c, between the array (see Figure 11) and their angle of attack. The value of the normal force acting on each array depends, of course, on its position in the field. Figure 19 shows the values of C_N for the 1st, 2nd and 5th arrays (from the upstream edge of the field) for head-on uniform winds. The magnitudes of the normal force on array No. 1 are approximately equal to their values in a single array. A drastic reduction in the magnitude of the normal forces on the 2nd and 5th arrays is observed. In some cases the direction of the normal force is reversed.

The magnitude of the forces acting on the 1st array can be reduced by building a fence or a barrier (zero porosity fence) upstream of the field. The effect of the fence depends on its porosity, height and distance. Figure 20 shows the effect of a 30 percent porosity fence and a zero porosity fence on the magnitude of the normal forces acting on the 1st and 2nd rows for different fence heights, and for an angle of attack $\alpha = 35°$. Similar results are obtained at different angles of attacks (see Figure 21).

The magnitude of the normal forces at the edge of an array, in case of head-on winds, is expected to be smaller than that of the forces acting on the center of the array. In case of side winds, however, the edges of the field and particularly the upstream corner will be exposed to higher loads. These forces can be reduced by a side fence and/or by different corner fence configurations. Figure 22 shows the corner fence configurations tested in this study. Their effect on the magnitude of the normal force for cornering winds is shown in Figure 23, which clearly exhibits the effect of properly designed fences on the normal forces at the field edges and corners.

Another way to reduce forces at the edge of the array field is to extend the array by an inexpensive stronger structure or by modifying the shape of the array edges. Several configurations, shown in Figure 24, have been studied. The fence configurations are also tabulated in Table 17. Their effect on the normal forces at the corner for $WD = 45°$ is shown in Figure 25 for $\alpha = 35°$ and $\alpha = 145°$.

An overall view of the results and the effect of the various parameters on the normal forces is shown in Figures 26-30. Figures 26 and 27 show the effect of the distance between the arrays for different angles of attack. Figure 28 summarizes the fence study for head-on winds. Figures 29-30 show the effect of the corner fences and the modifications of the array edges. All test configurations investigated for this study are listed in Table 18.

4.3 Flow Visualization

Flow visualization was used in this study to explore the structure of the flow in the array field and to obtain a better understanding of the force and pressure measurements.

Figure 31a shows the wake behind the first array in the field and behind an array in the center of the field. Clear flow separation is observed for this angle of attack and spacing. Figures 31b and 31c show the structure and the nature of the flow at different points between the arrays.

Figure 32 shows two corner fence configurations and their effect on the flow structure near the fence.

5. CONCLUSIONS

Wind loadings on photovoltaic arrays in a large array field were measured on 1:24 and 1:12 scale wind-tunnel models. The dimensionless pressure and force coefficients measured are independent of the Reynolds number and can therefore be used for the design of prototype arrays.

Considerable differences were found between the normal force coefficients for uniform and nonuniform velocity fields. The arrays at the edges and corners of the field will usually be exposed to much larger forces than the arrays in the interior of the field. These forces can be considerably reduced, however, by fences and barriers. Data is presented which make it possible to design the prototype array field and fences for given atmospheric winds.

6. REFERENCES

1. American National Standards Institute, American National Standard Building Code Requirements for Minimum Design Loads in Buildings and Other Structures, ANSI Standard A58.1, 1972.

2. Miller, R. D. and Zimmerman, D., Wind Loads on Flat Plate Photovoltaic Array Fields, Boeing Engineering and Construction Report No. DOE/JPLG54833-79/2, Seattle, Washington 98124, September 1979.

3. Cermak, J. E., Aerodynamics of Buildings, Annual Review of Fluid Mechanics, Vol. 8, 1976.

4. Cermak, J. E., Laboratory Simulation of the Atmospheric Boundary Layer, AIAA Jl., Vol. 9, September 1971.

5. Cermak, J. E., Applications of Fluid Mechanics to Wind Engineering, A Freeman Scholar Lecture, ASME Jl. of Fluids Engineering, Vol. 97, No. 1, March 1975.

6. Bearman, P. W., Turbulence Effects on Bluff Body Mean Flow, Third U.S. National Conference on Wind Engineering Research, pp. 265-272, 1978.

7. Bearman, P. W., An Investigation of the Forces on Flat Plates Normal to a Turbulent Flow, Jl. Fluid Mechanics, Vol. 46, pp. 177-198, 1971.

8. Nakamura, Y. and Tomonari, Y., The Effect of Turbulence on the Drag of Rectangular Prisms, Transactions Japan Society of Aeronautical and Space Science, Vol. 19, pp. 81-86, 1976.

9. Harris, R. I., The Nature of the Wind, Modern Design for Wind Sensitive Structures, Paper 3, 1971.

10. Davenport, A. G., The Spectrum of Horizontal Gustiness Near the Ground, Quarterly Jl., Royal Meteorological Society, Vol. 81, pp. 194-211, 1961.

FIGURES

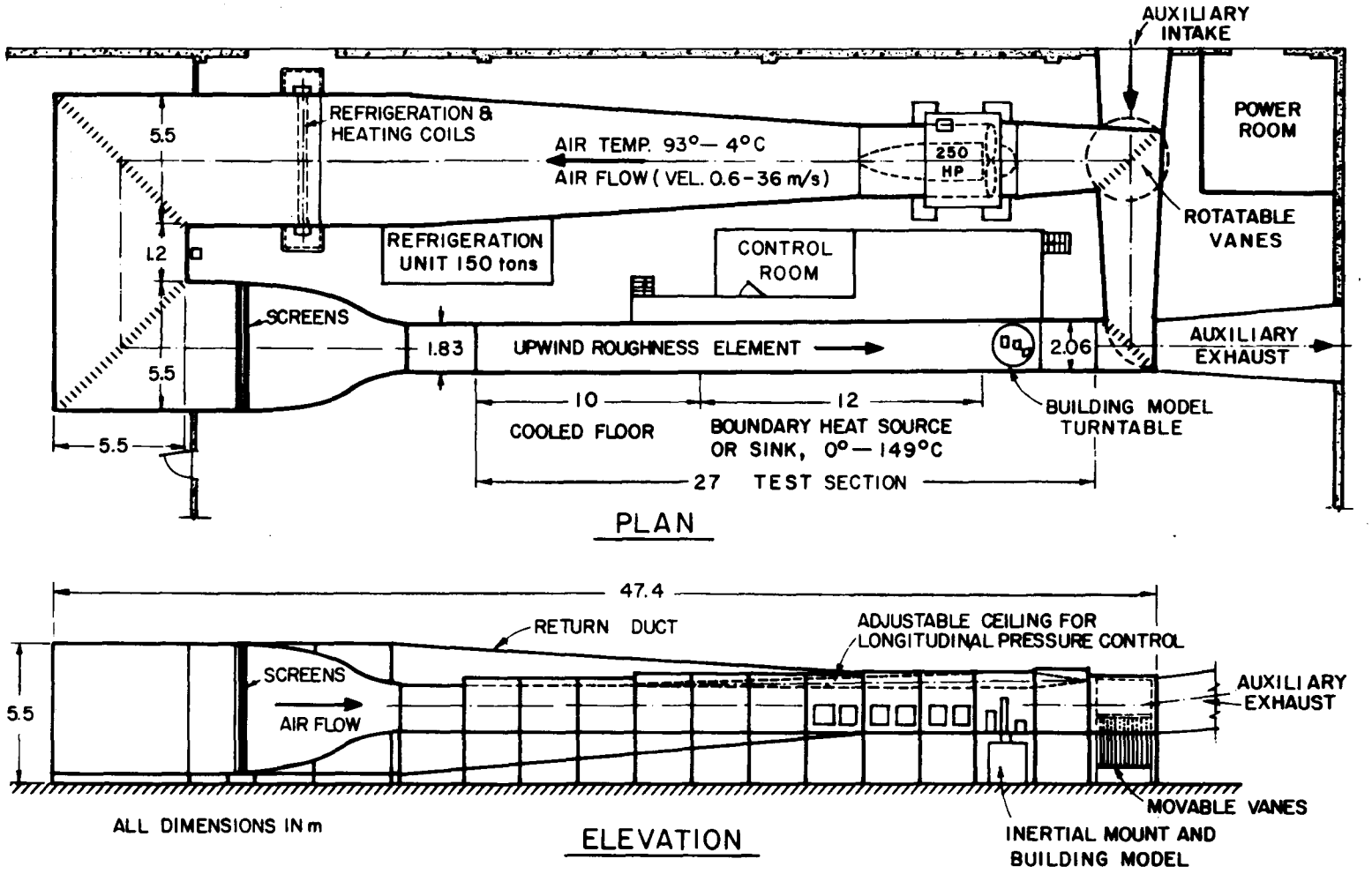

Figure 1. Meteorological Wind Tunnel

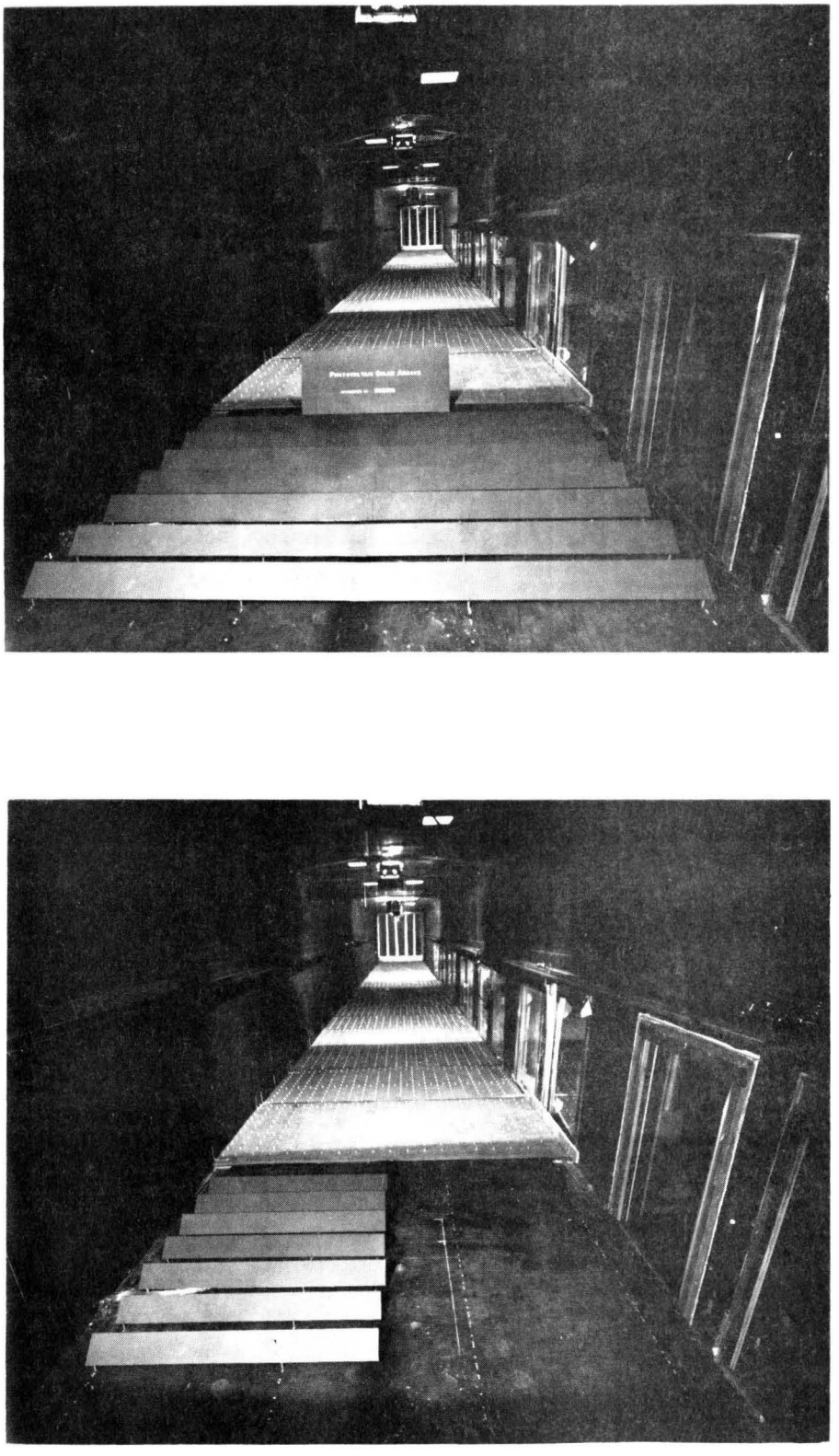

Figure 2. Array Field Models in Meteorological Wind Tunnel

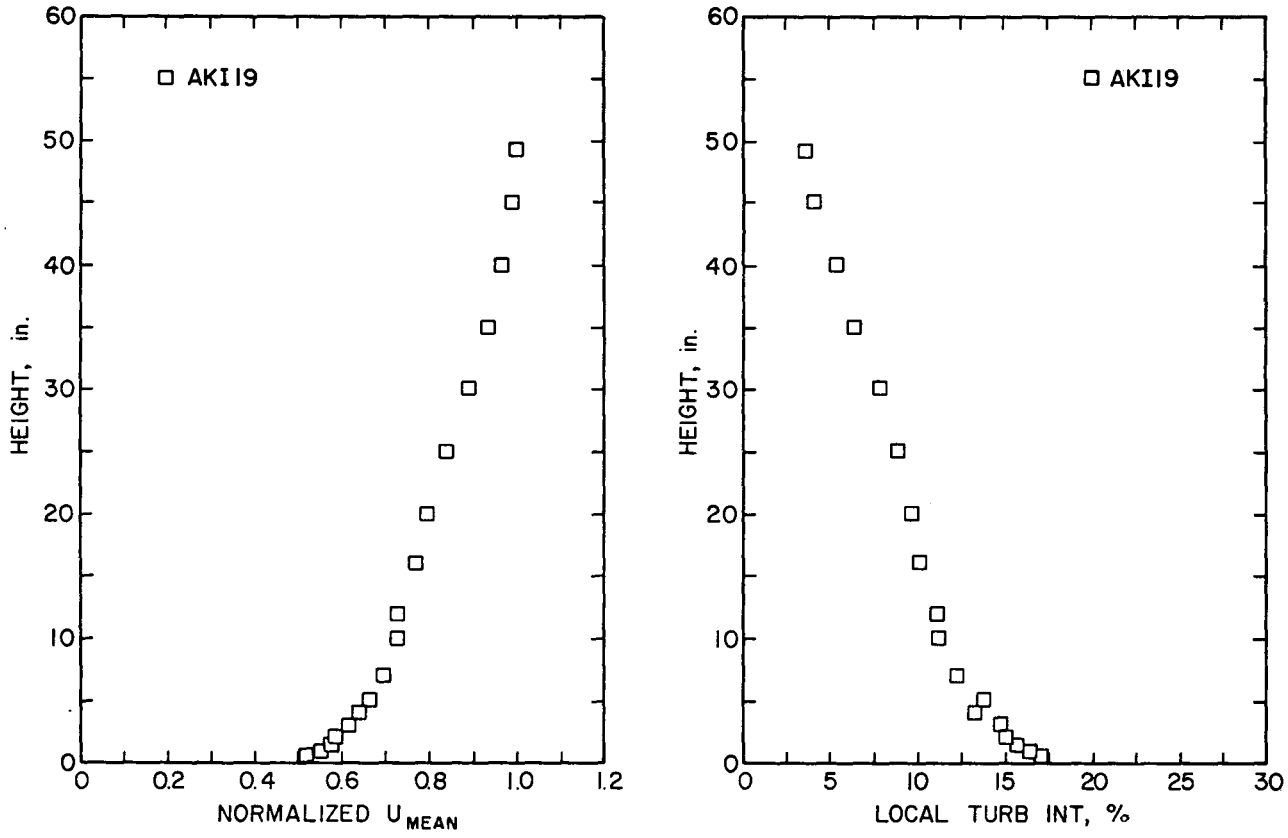

Figure 3. Mean Velocity and Turbulence Distribution in Nonuniform Flow

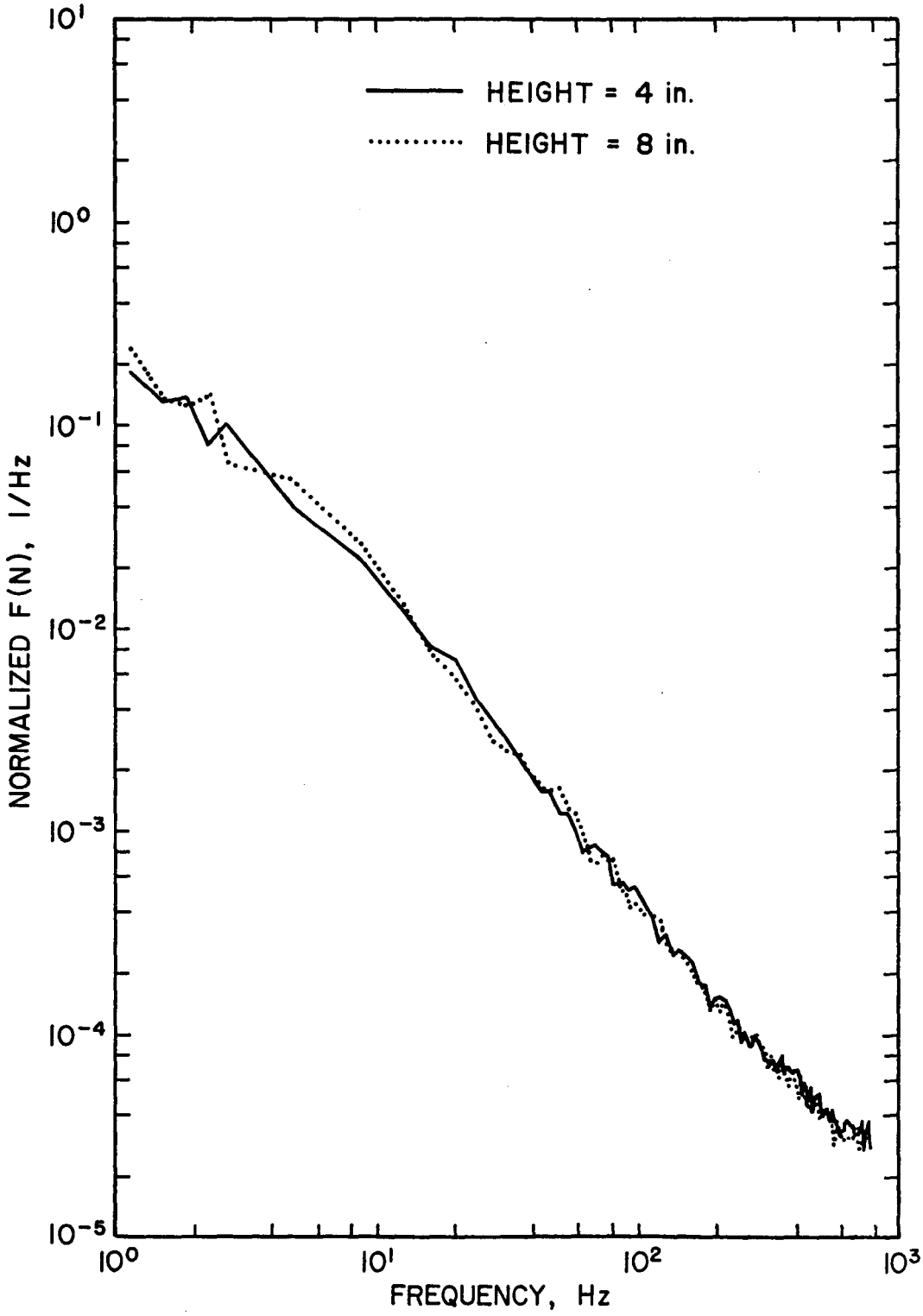

Figure 4. One Dimensional Velocity Spectra in Nonuniform Flow

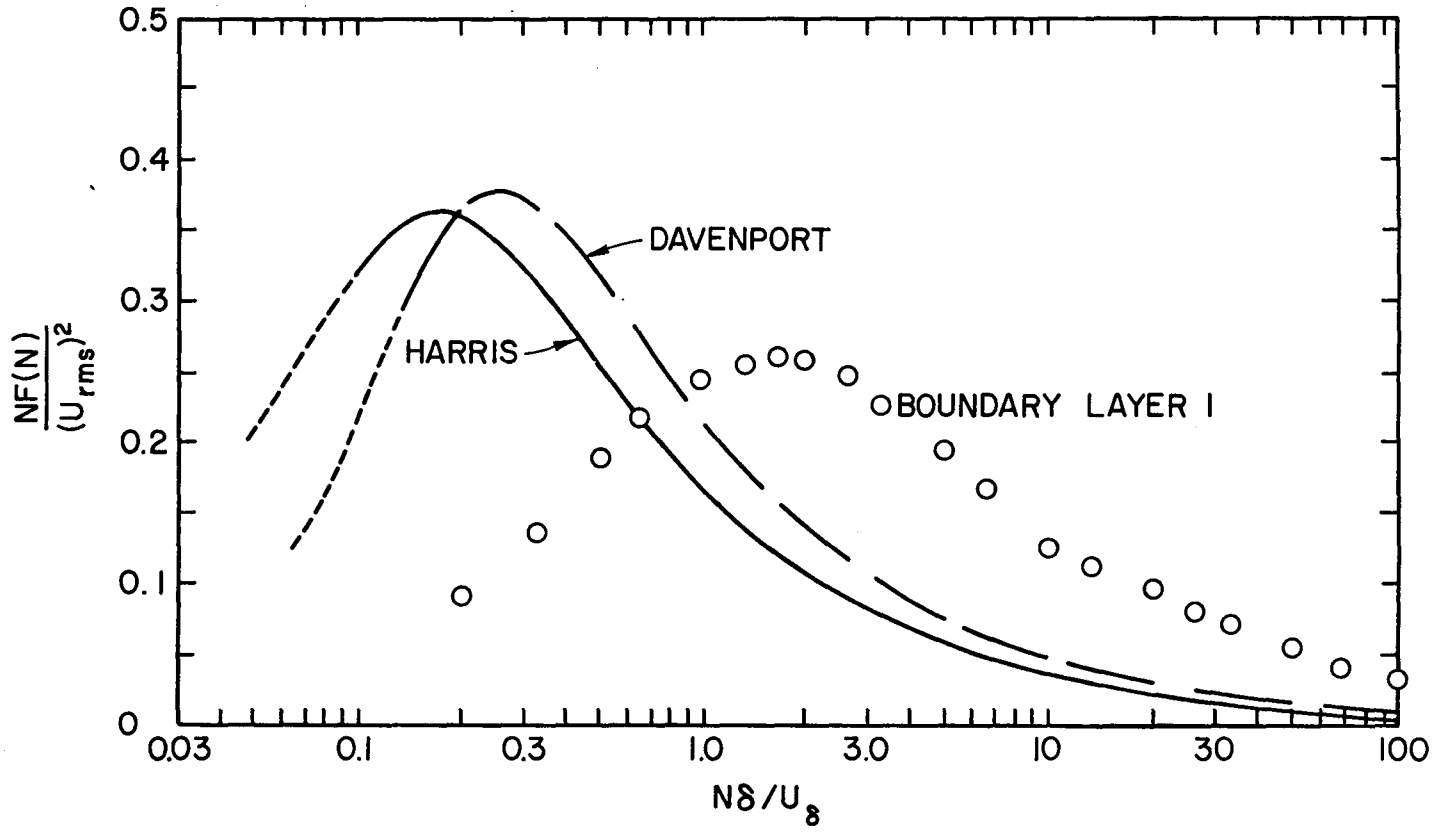

Figure 5. Turbulence Spectra in Nonuniform Flow (BL1) Compared to Atmospheric Spectra

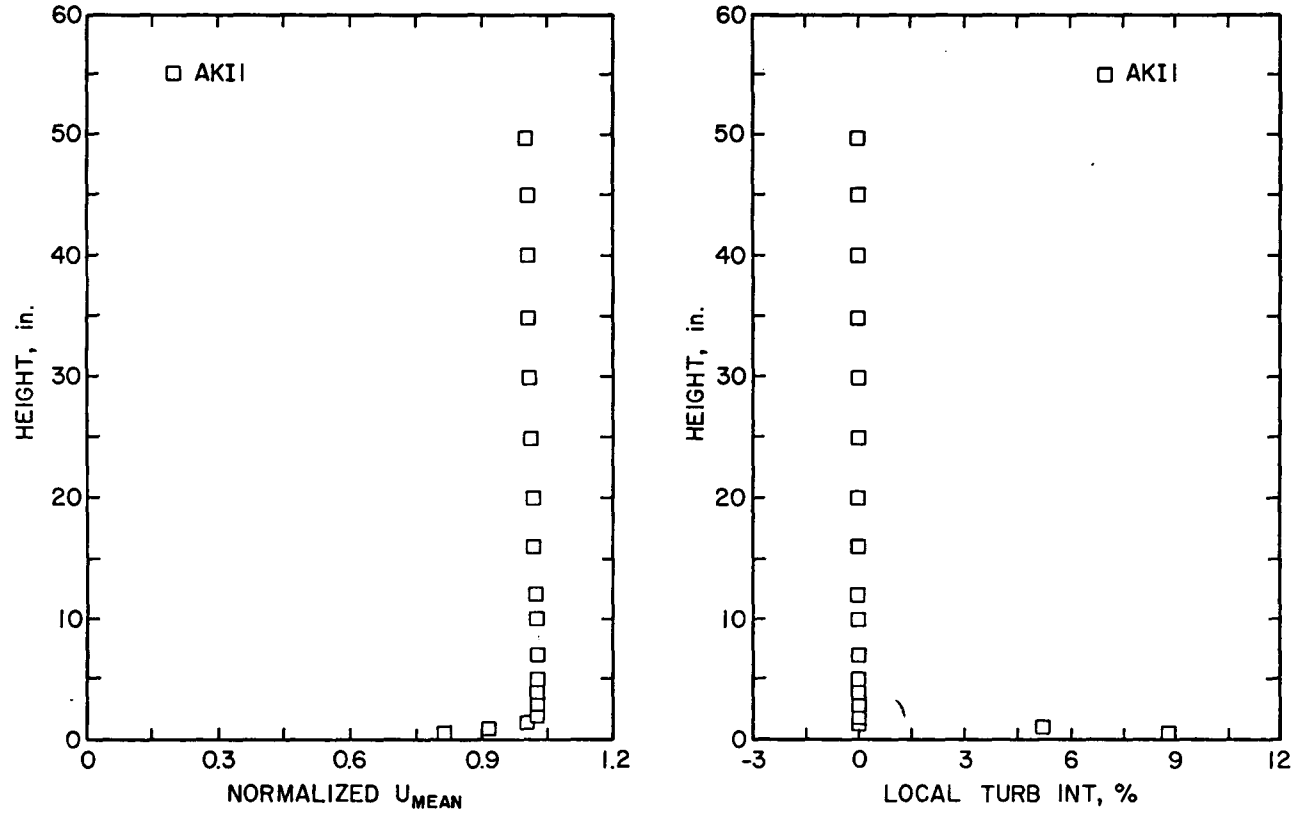

Figure 6. Mean Velocity and Turbulence Distribution in Uniform Flow

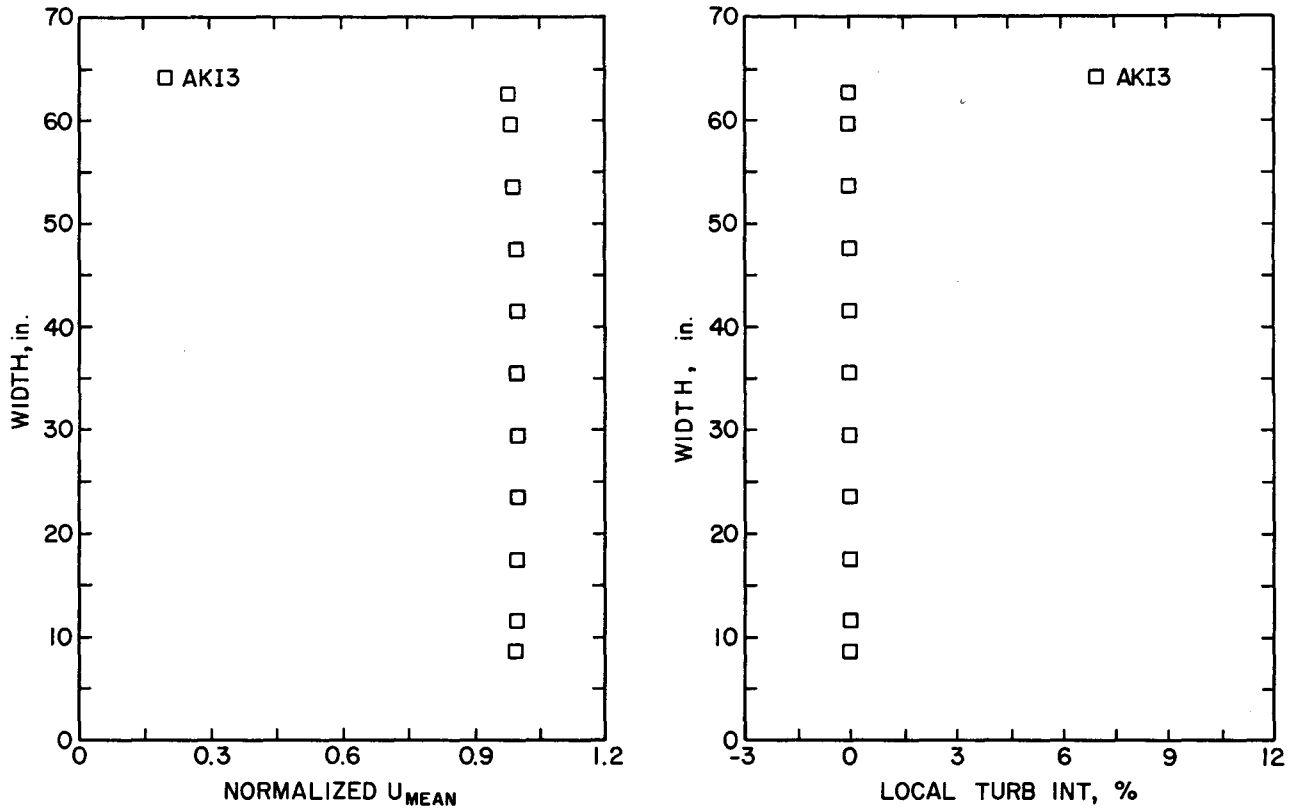

Figure 7. Typical Horizontal Velocity Distribution across Meteorological Wind Tunnel

Figure 8. 1:12 Scale Models in Meteorological Wind Tunnel

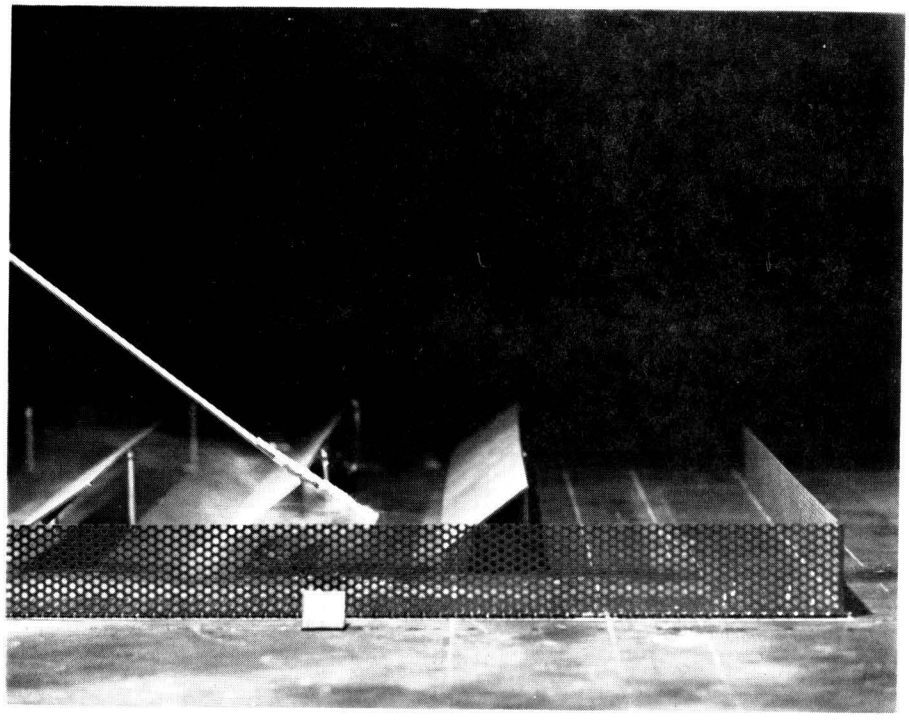

Figure 9. Photograph of Standard Corner Fence

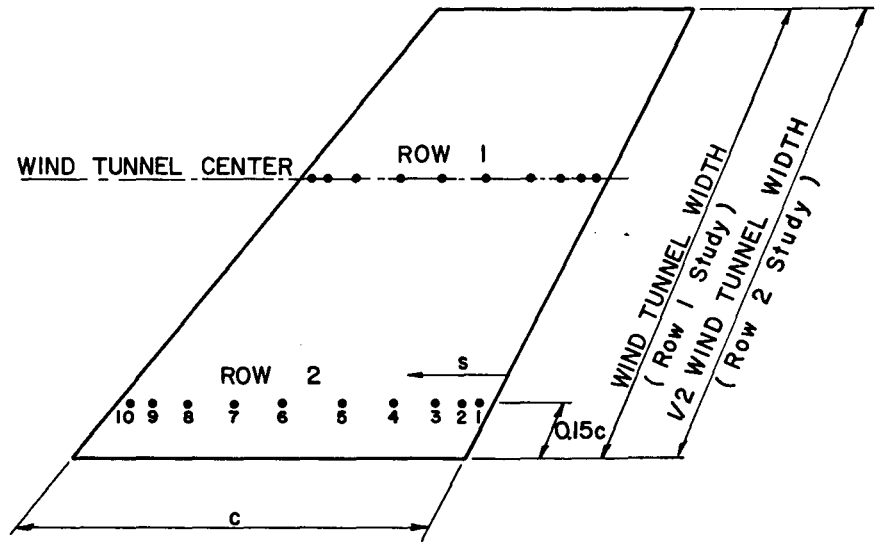

TAP LOCATIONS - FRACTION OF CHORD s/c

	1	2	3	4	5	6	7	8	9	10
UPSTREAM SURFACE	0.052	0.102	0.172	0.272	0.432	0.592	0.752	0.852	0.922	0.972
DOWNSTREAM SURFACE	0.028	0.078	0.148	0.248	0.408	0.568	0.728	0.828	0.898	0.948

Figure 10. Position of Pressure Taps on Instrumented Model

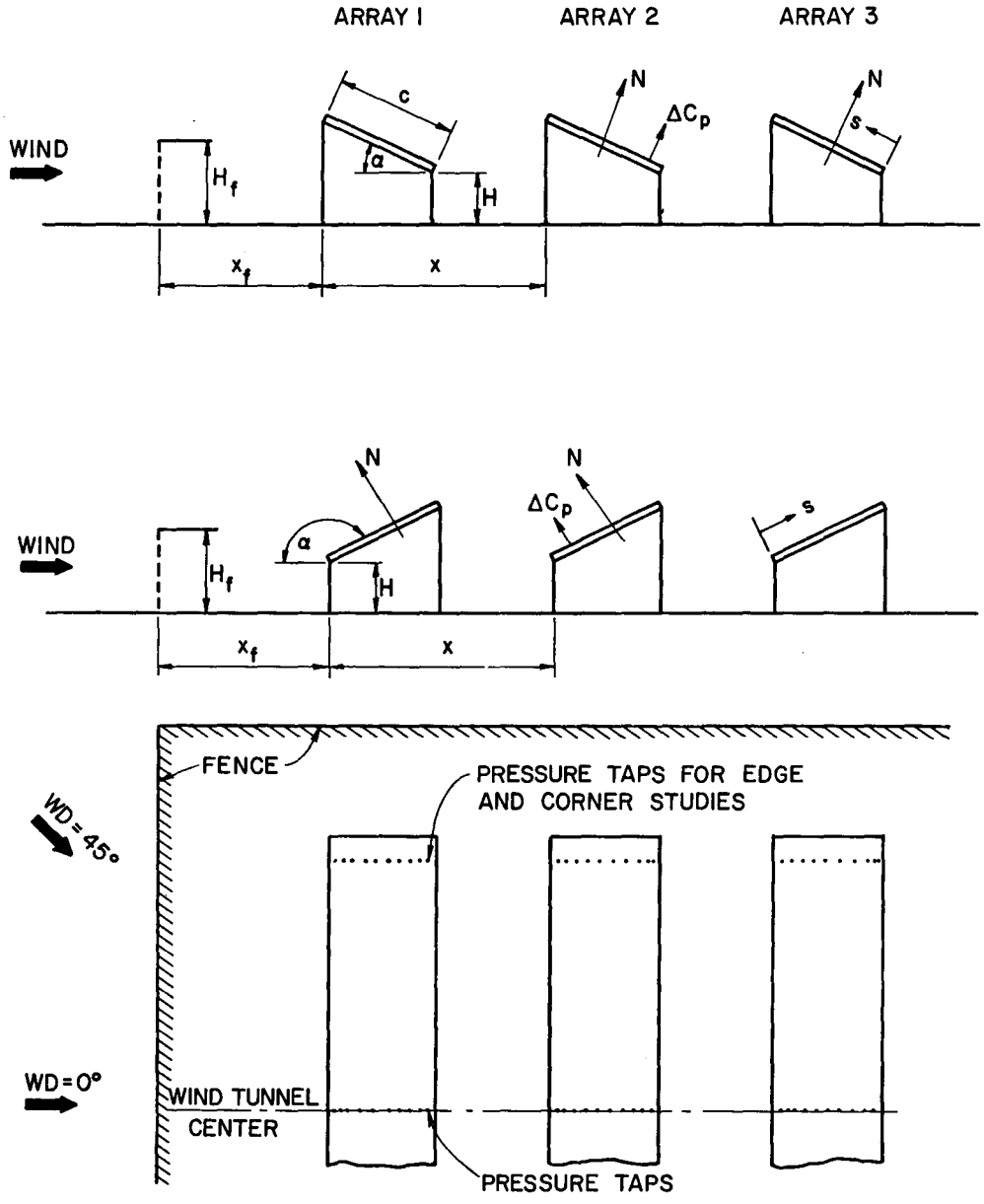

Figure 11. Schematic Description of Array Field

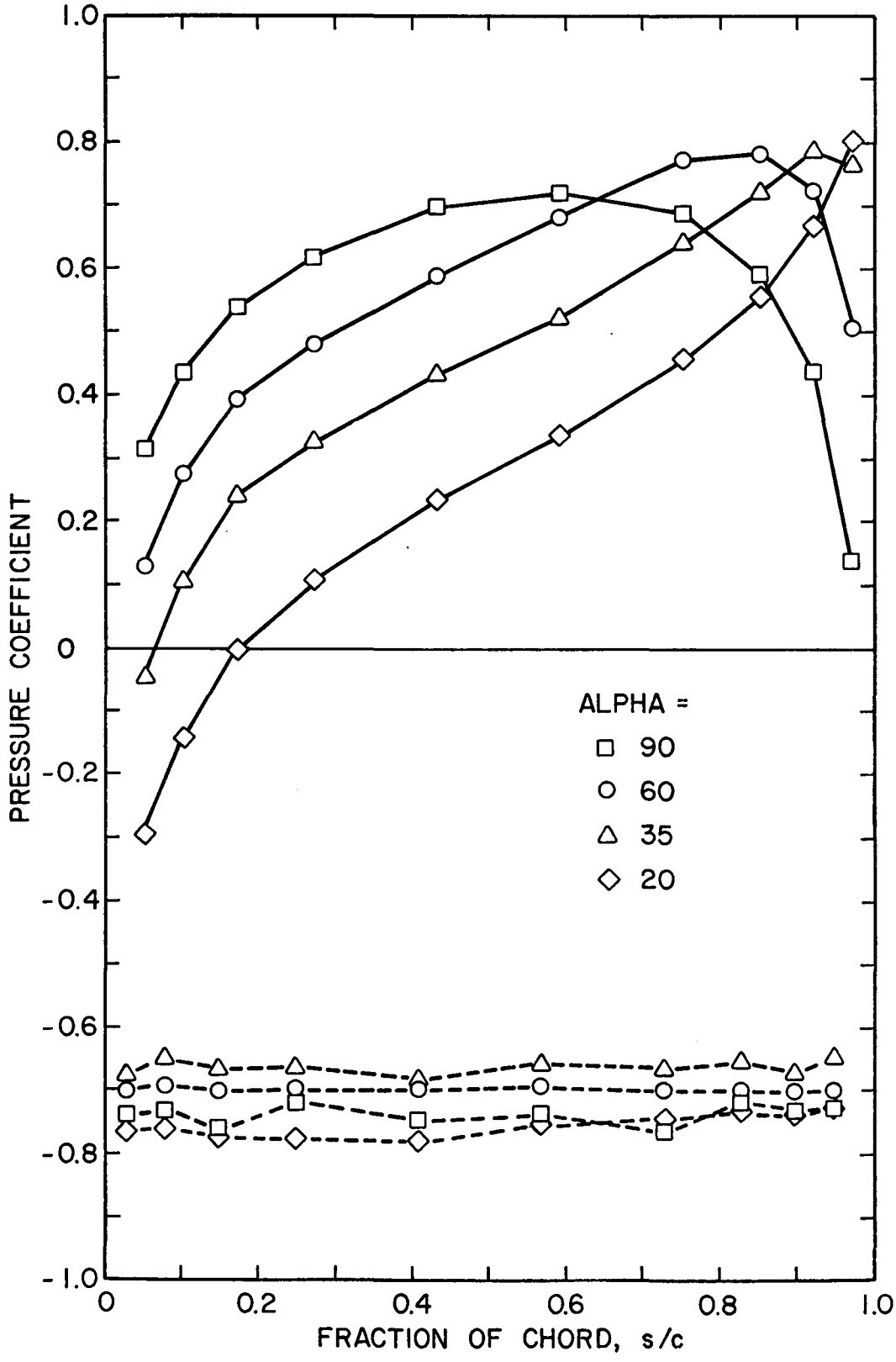

Figure 12. Front and Back Pressures on a Single Array in Uniform Flow, WD = 0°, H/c = 0.25, α = 20°, 35°, 60° and 90°

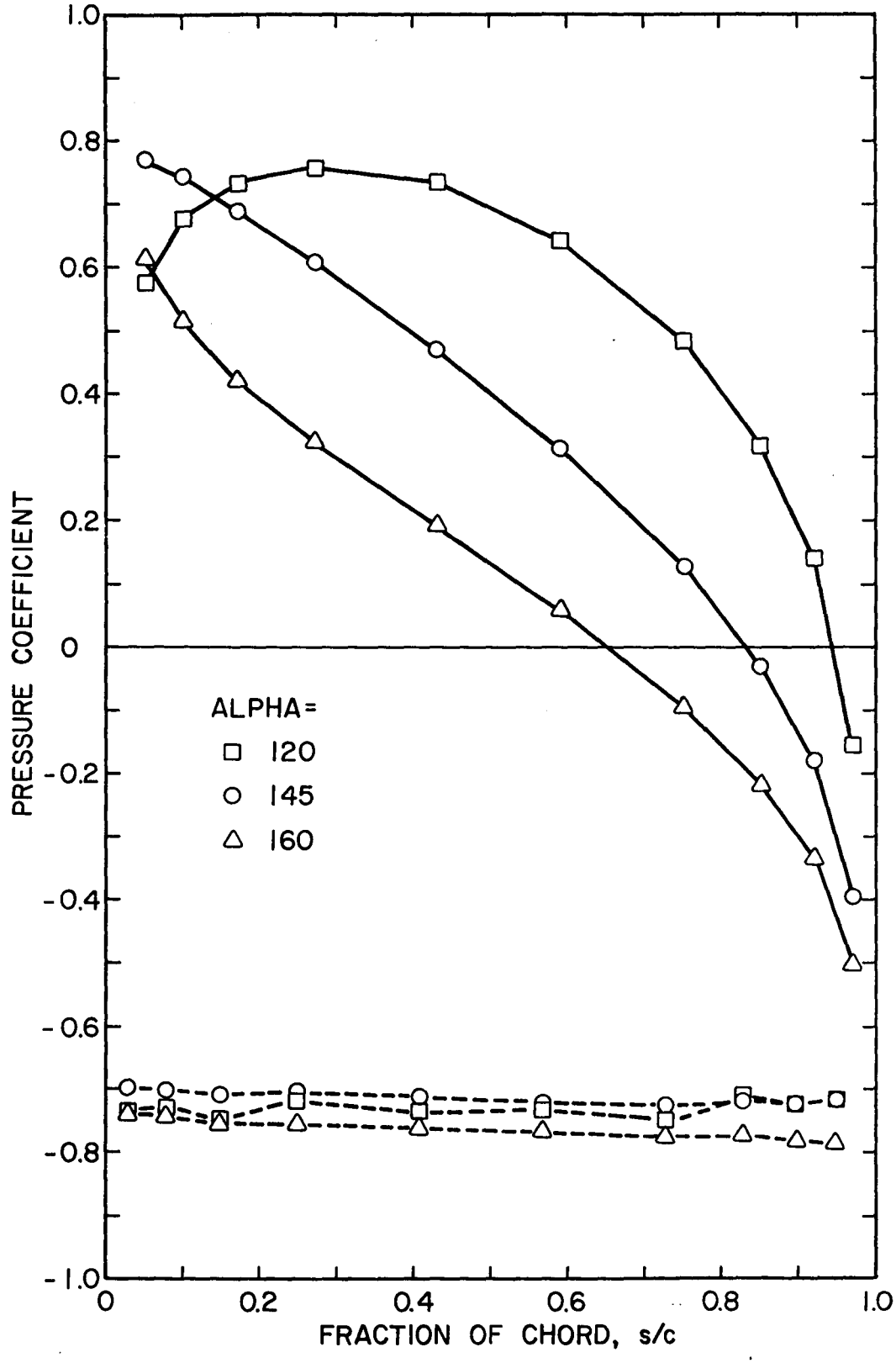

Figure 13. Front and Back Pressures on a Single Array in Uniform Flow, WD = 0°, H/c = 0.25, α = 120°, 145° and 160°

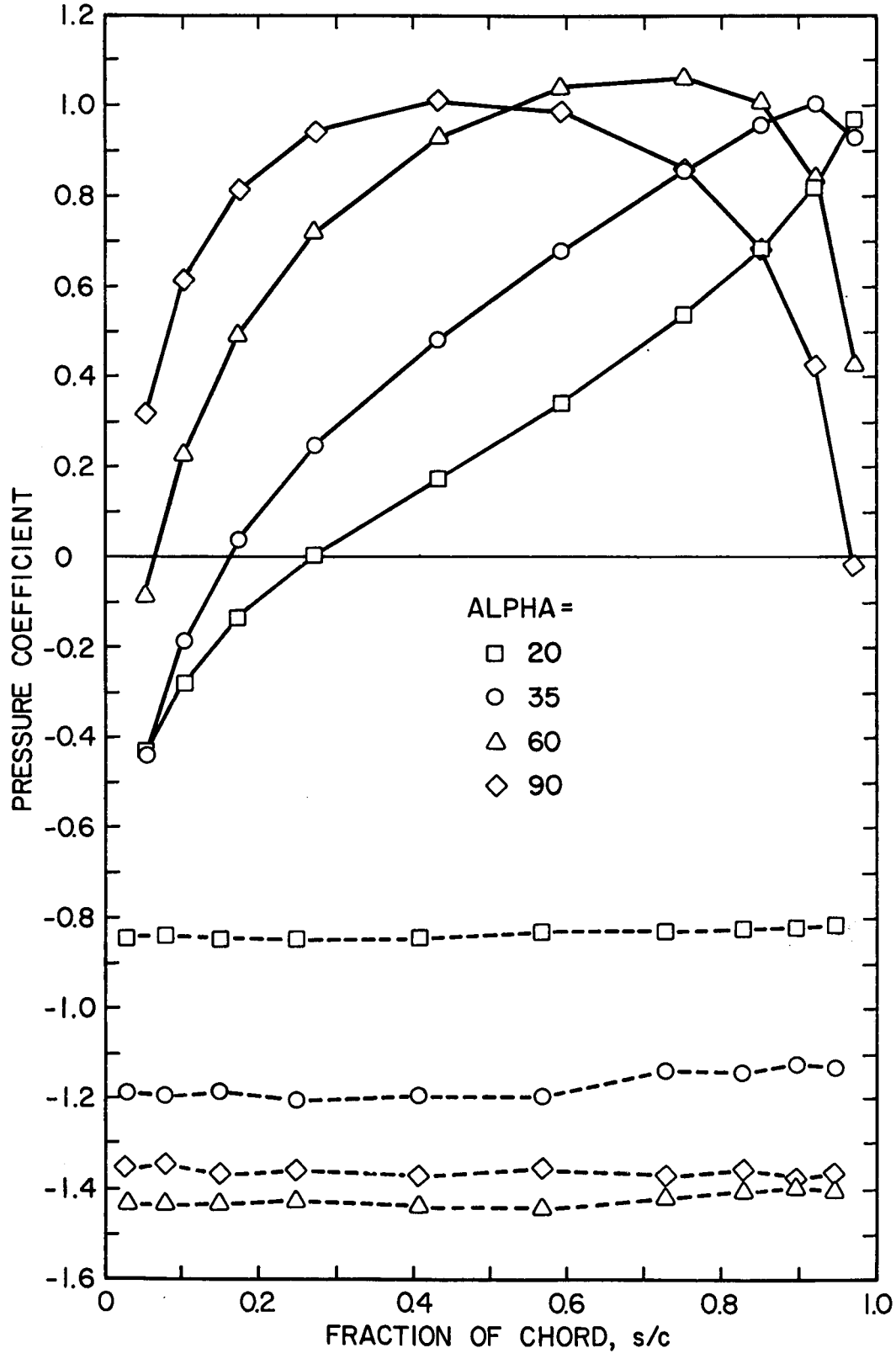

Figure 14. Front and Back Pressures on a Single Array in Uniform Flow, WD = 0°, H/c = infinity, α = 20°, 30°, 60°, and 90°

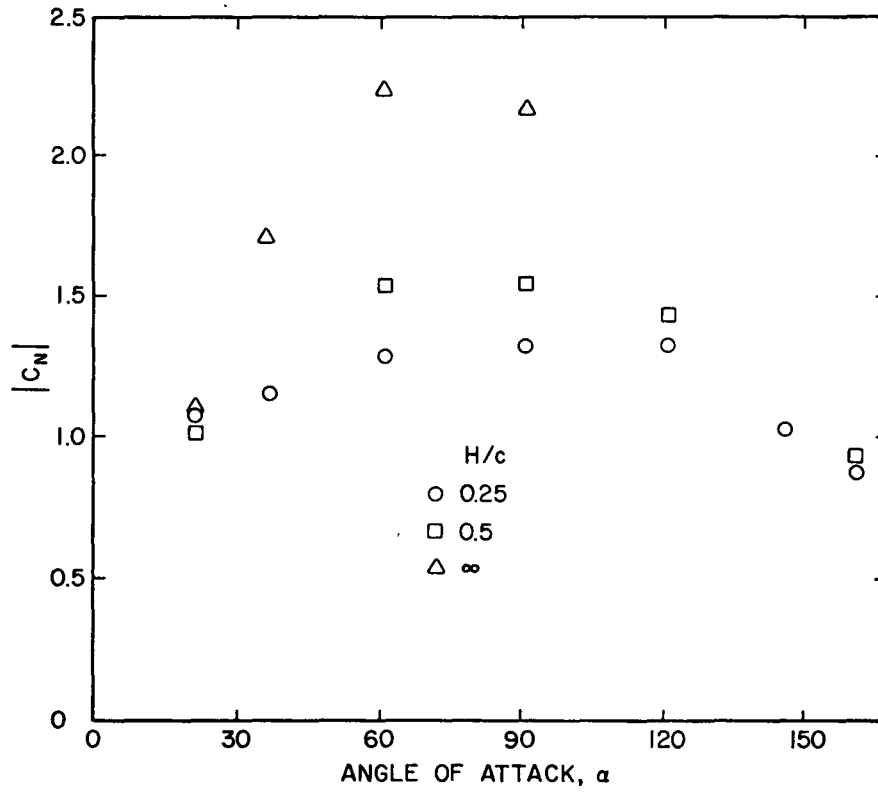

Figure 15. Absolute Values of Normal Force Coefficients on a Single Array in Uniform Flow, WD = 0°

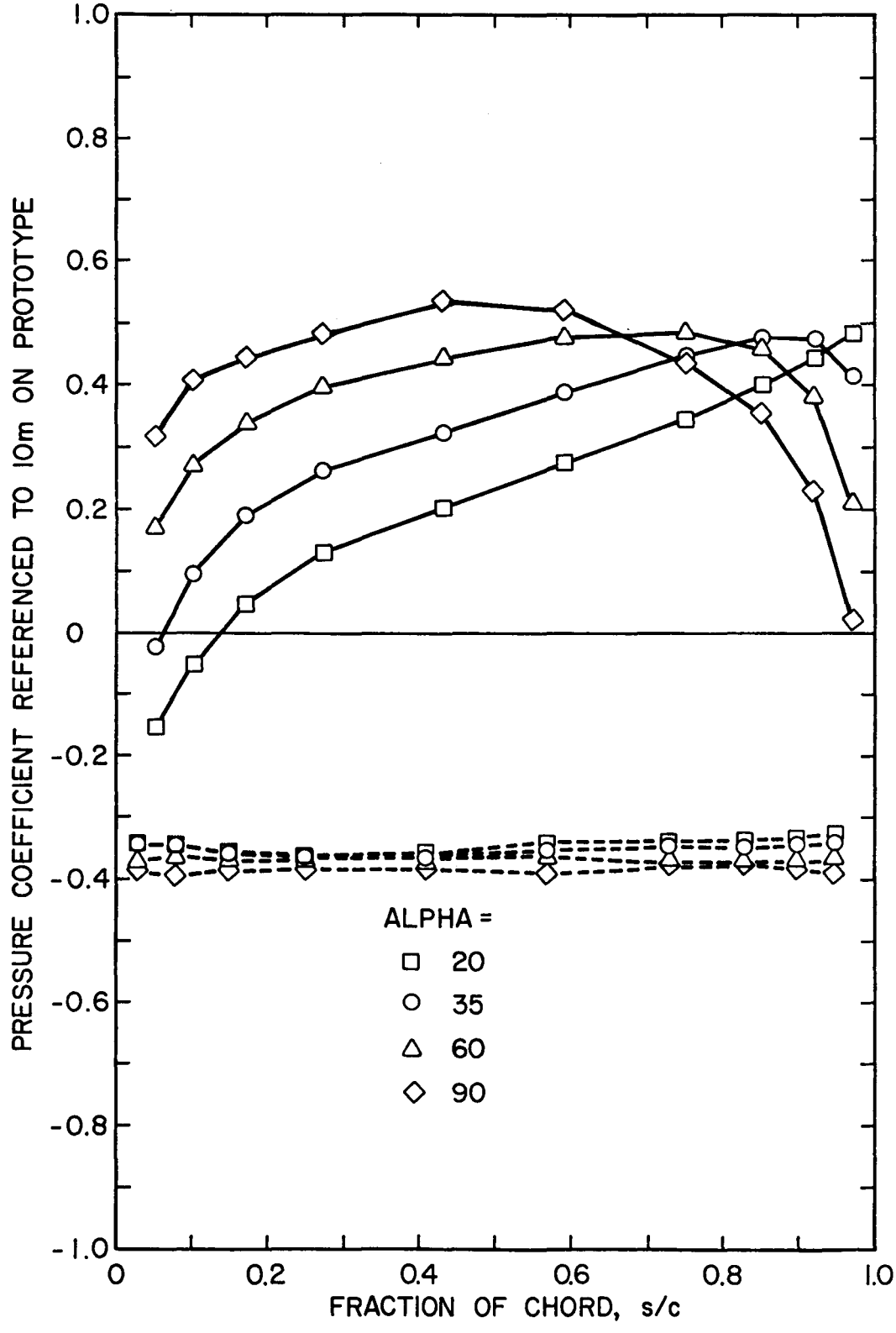

Figure 16. Front and Back Pressures on a Single Array in Nonuniform Flow, WD = 0°, H/c = 0.25, α = 20°, 30°, 60° and 90°

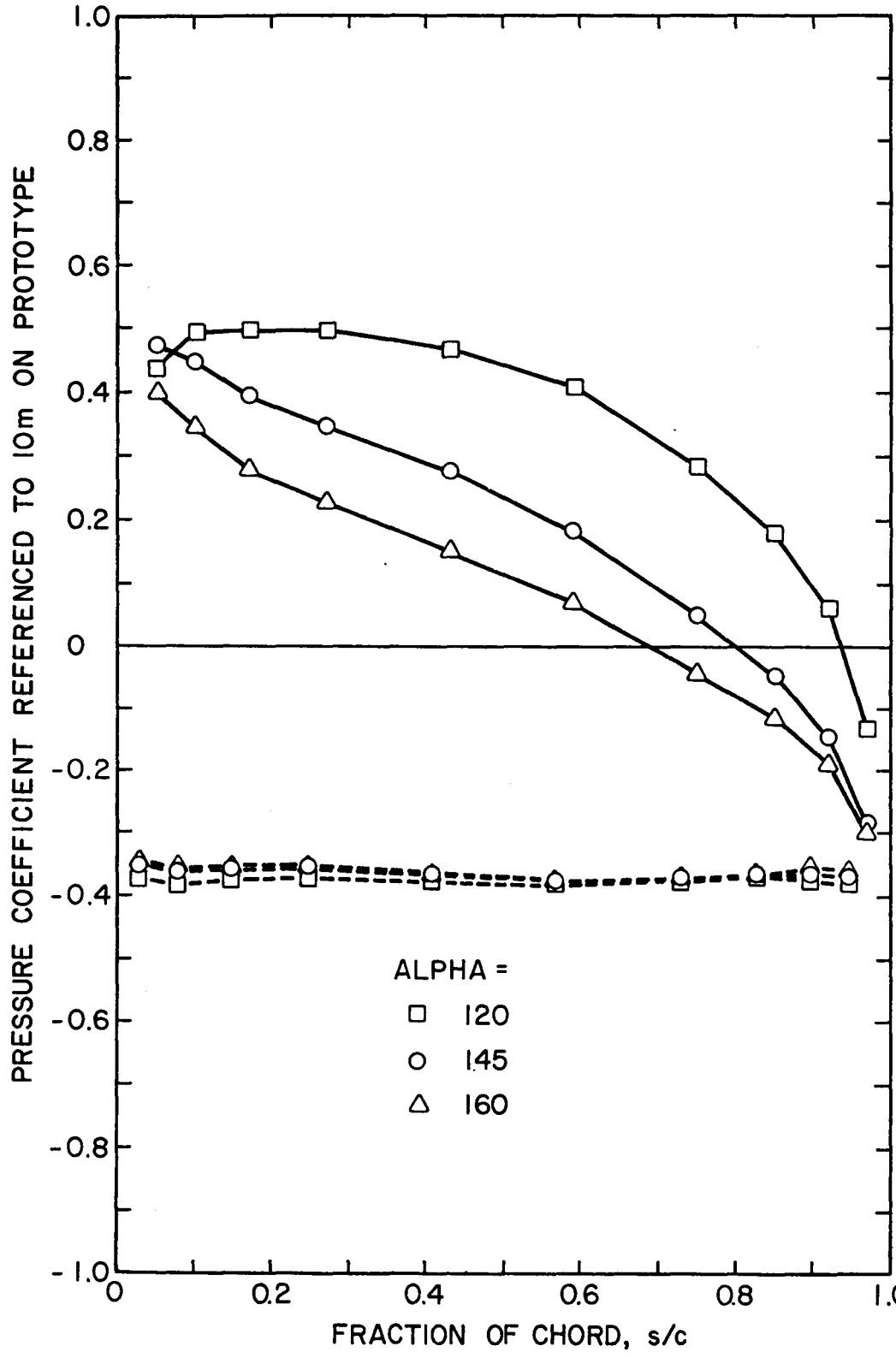

Figure 17. Front and Back Pressures on a Single Array in Nonuniform Flow, WD = 0°, H/c = 0.25, α = 120°, 145° and 160°

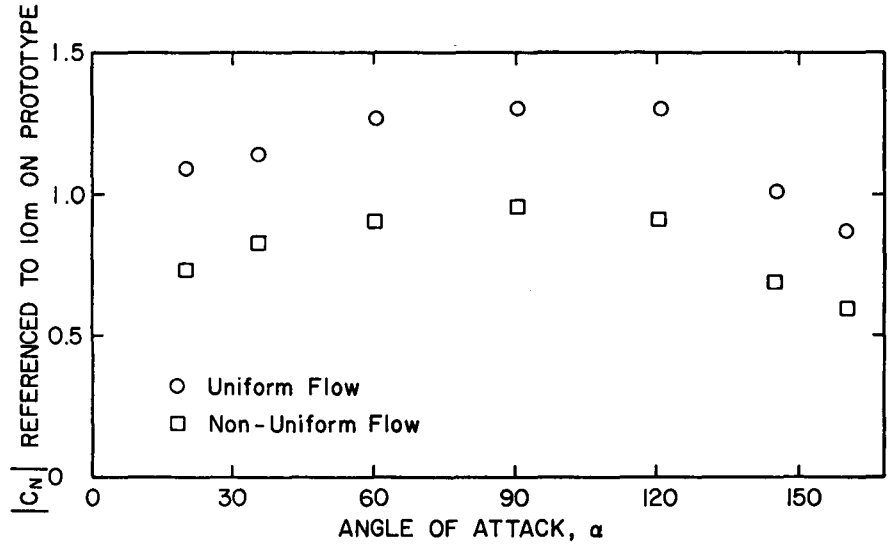

Figure 18. Absolute Values of Normal Force Coefficients on a Single Array in Nonuniform and Uniform Flows, WD = 0°, H/c = 0.25

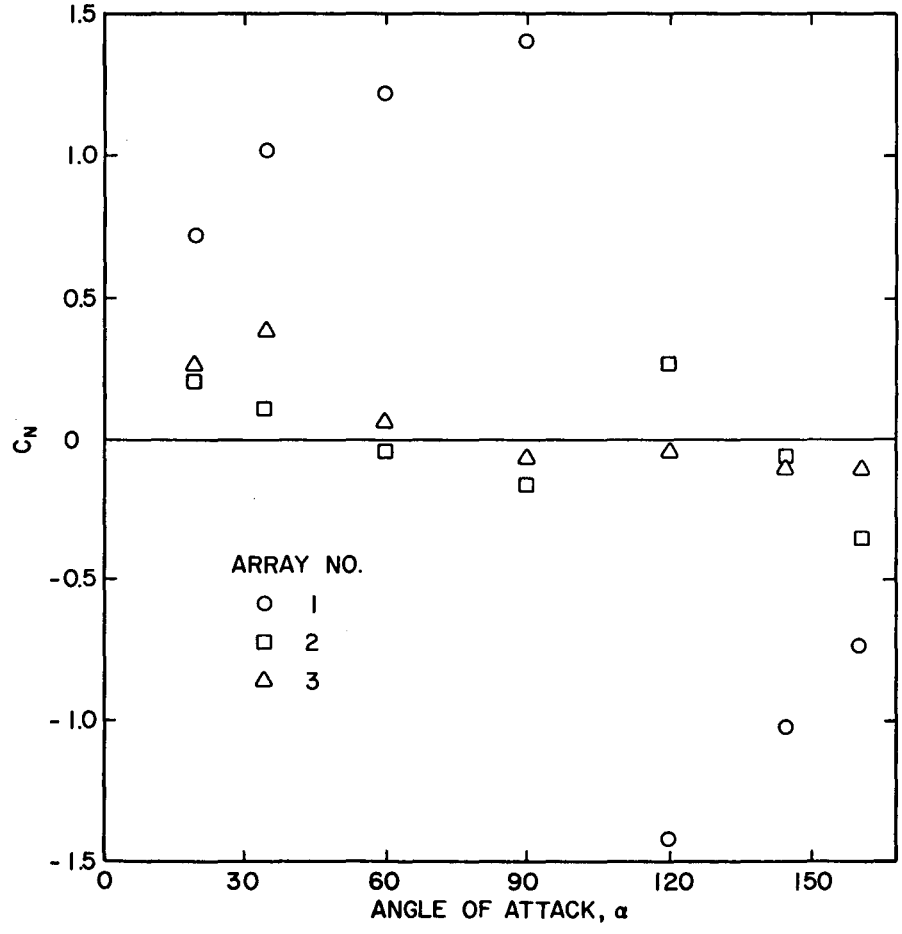

Figure 19. Normal Force Coefficients for an Array Field in Uniform Flow, WD = 0°, x/c = 2.0, H/c = 0.25, No Fence

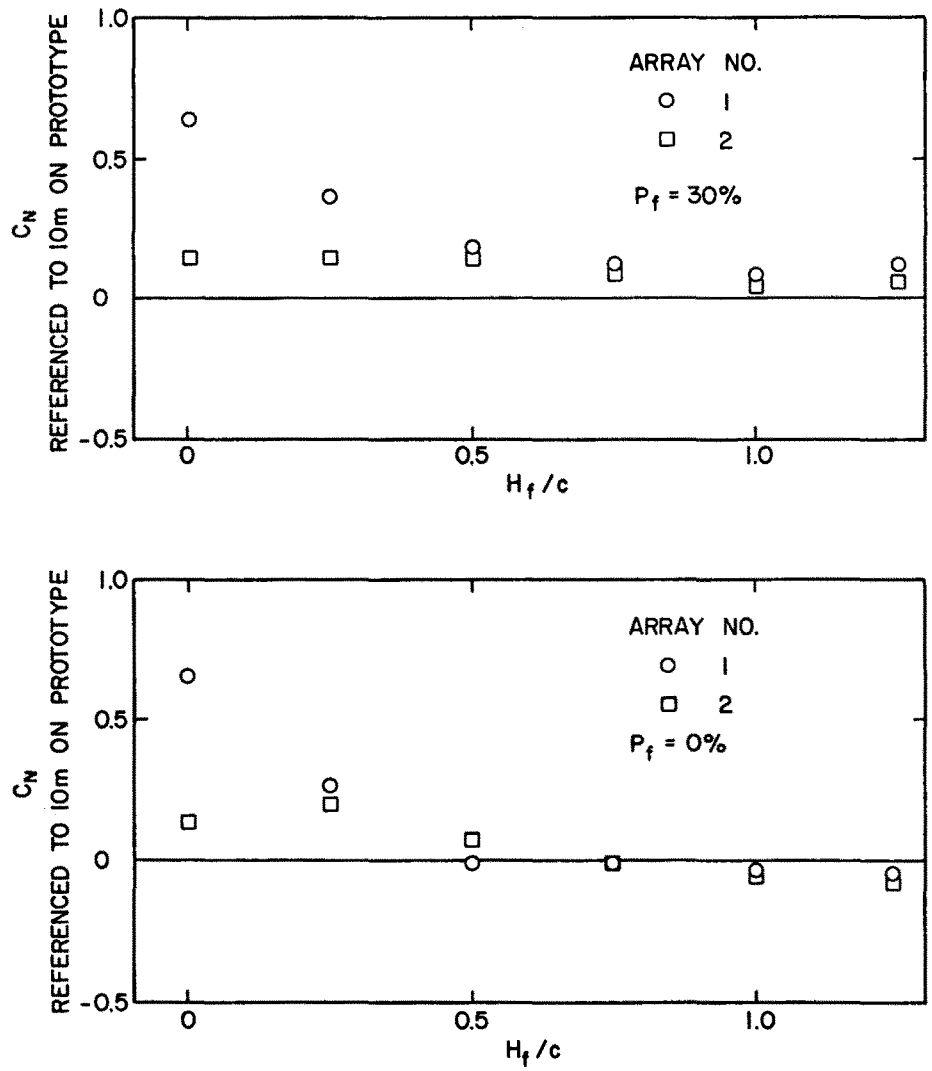

Figure 20. Normal Force Coefficients for an Array Field with a Fence of Various Height and Porosity, WD = 0°, x/c = 2.0, H/c = 0.25, α = 35°

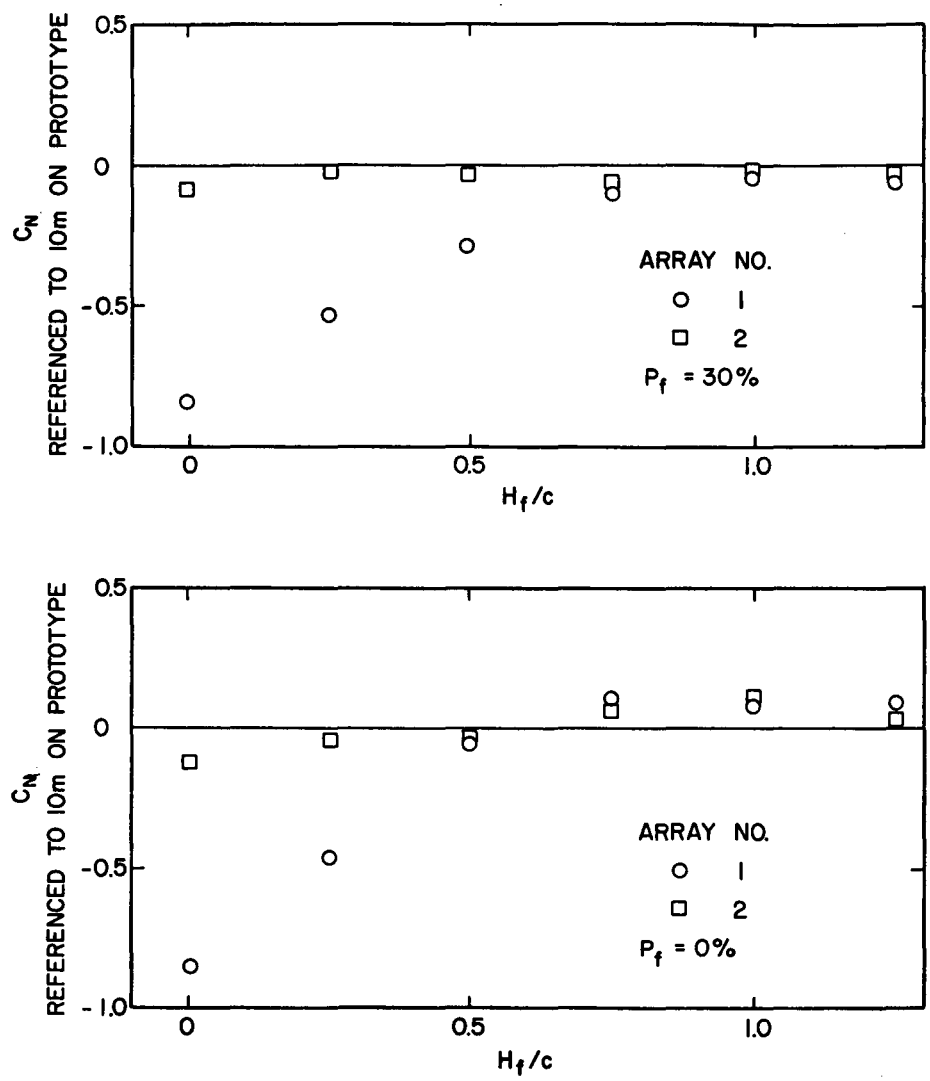

Figure 21. Normal Force Coefficients for an Array Field with a Fence of various Height and Porosity, WD = 0°, x/c = 2-0, H/c = 0.25, α = 145°

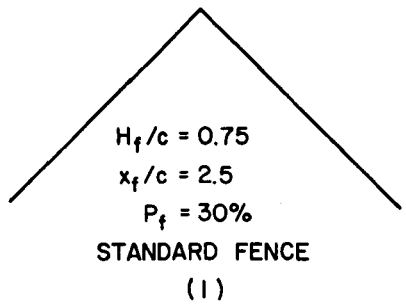

STANDARD FENCE
(1)

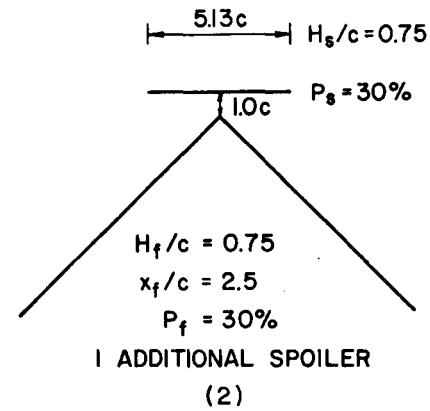

1 ADDITIONAL SPOILER
(2)

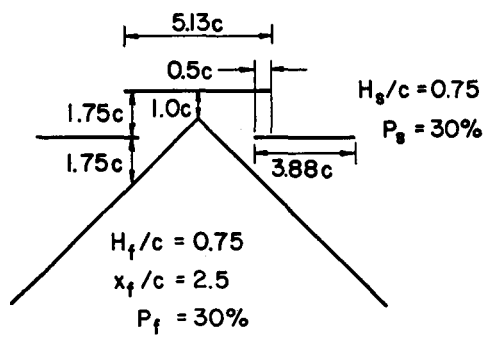

3 ADDITIONAL SPOILERS
(3)

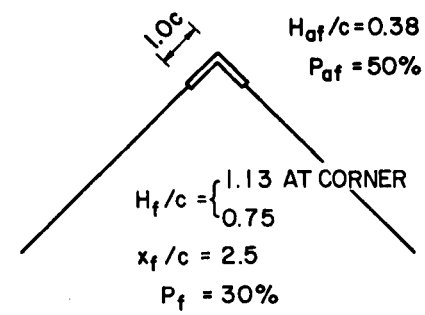

ADDITIONAL FENCE AT CORNER
(4)

Figure 22. Corner Fence Configurations

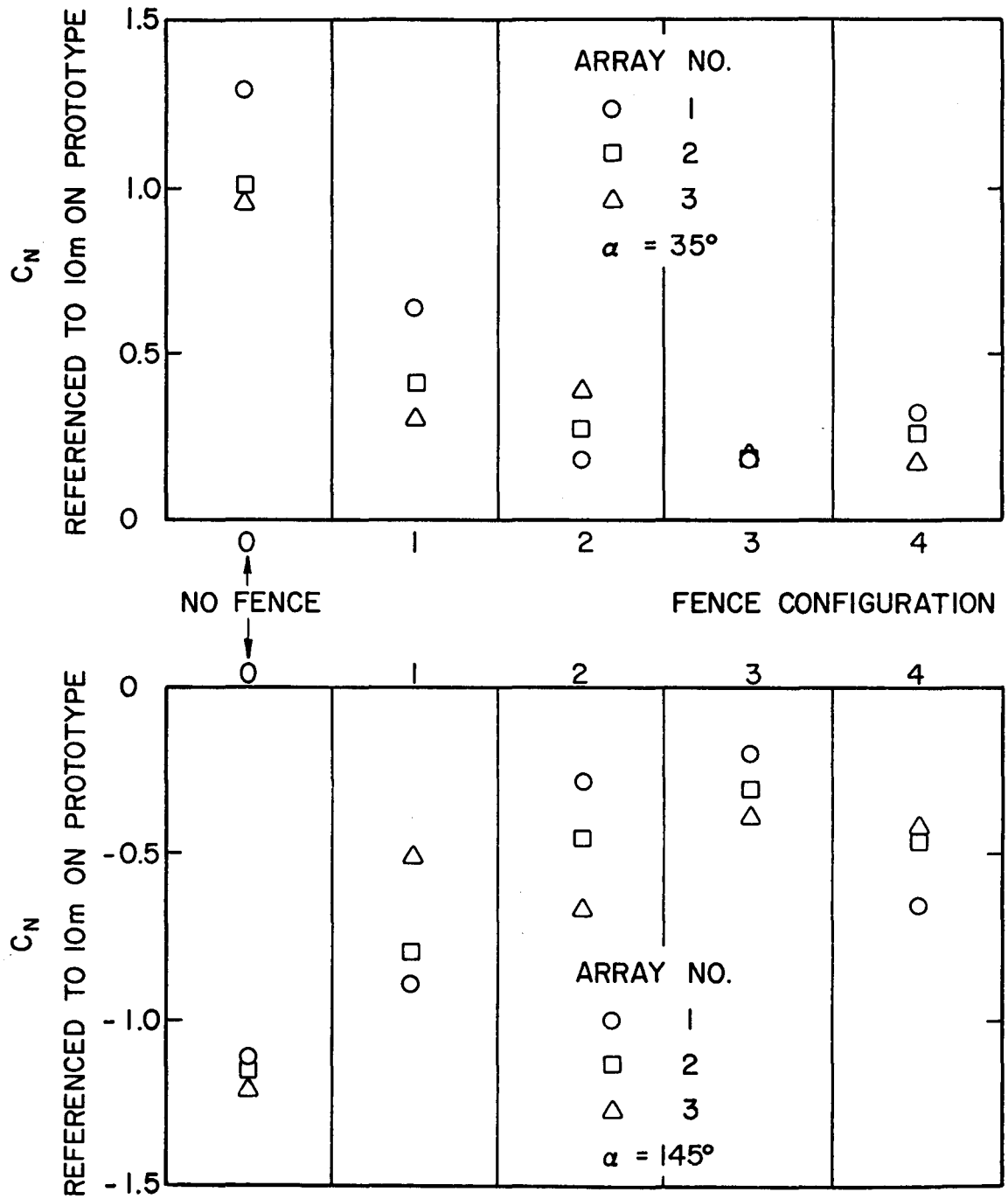

Figure 23. Normal Force Coefficients for an Array Field with Various Fence Configurations; WD = 45°, x/c = 2.0, H/c = 0.25, MC = 0

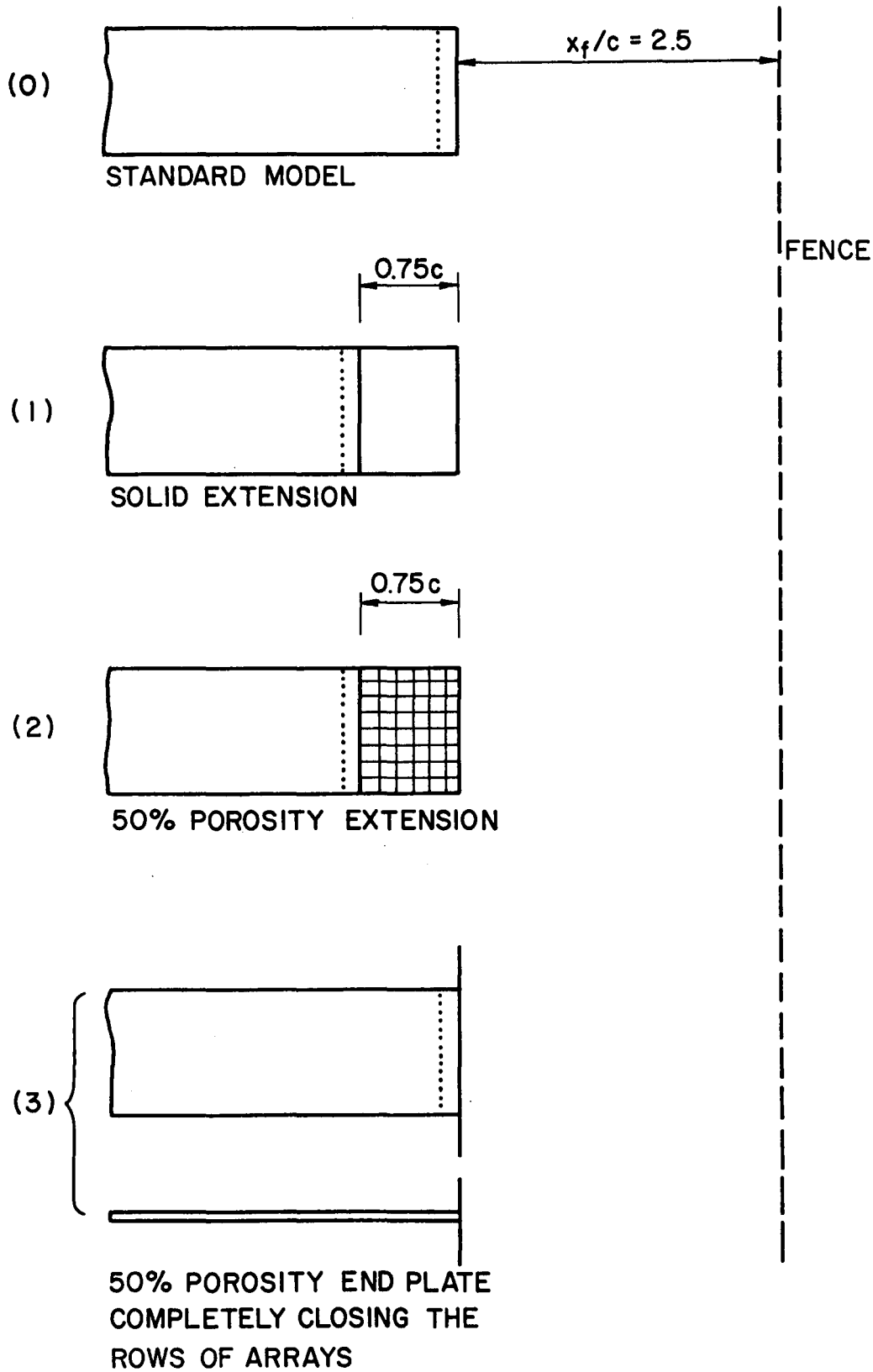

Figure 24. Model Configurations

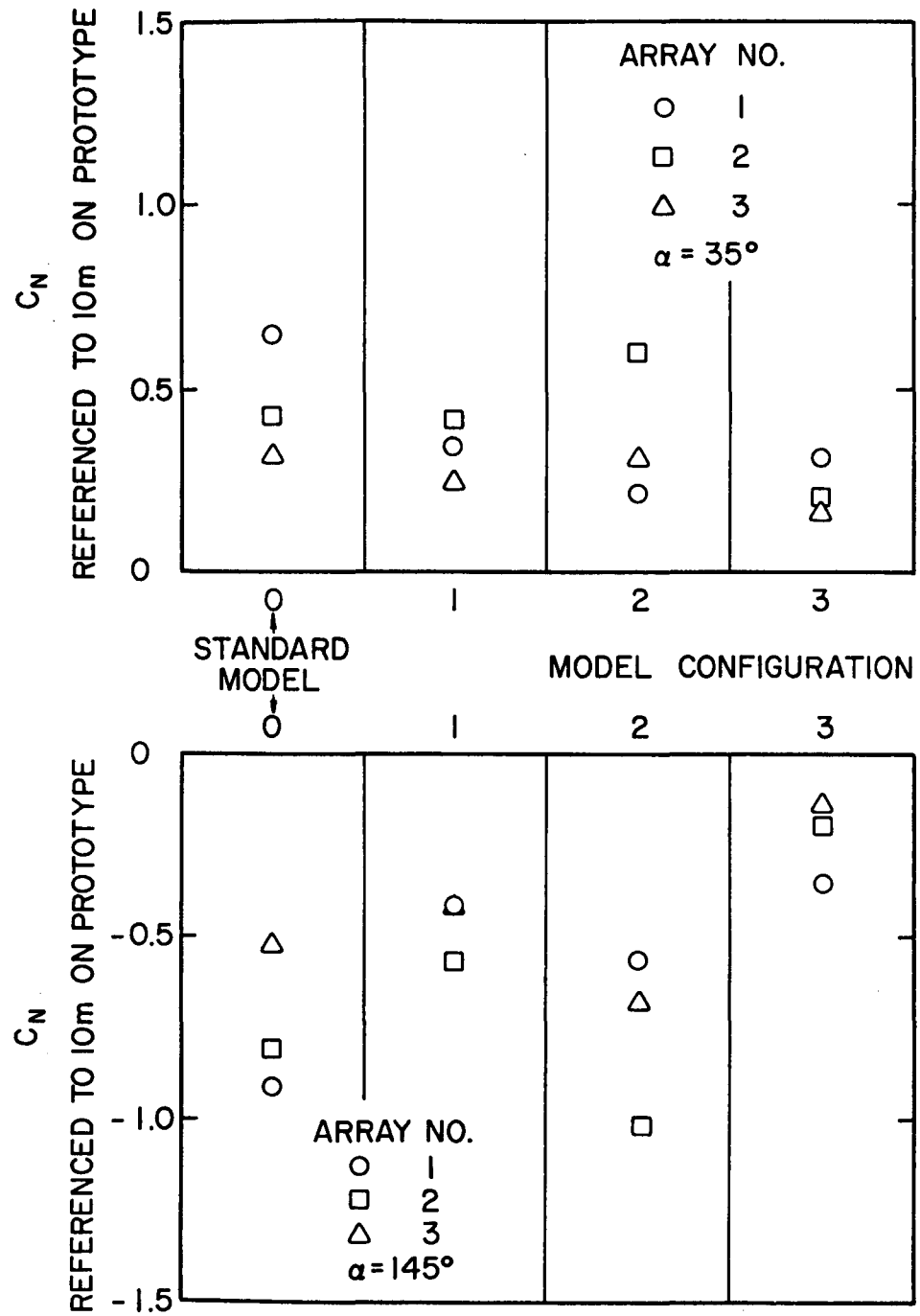

Figure 25. Normal Force Coefficients for an Array Field with Various Model Configurations, WD = 45°, x/c = 2.0, H/c = 0.25, FC = 1

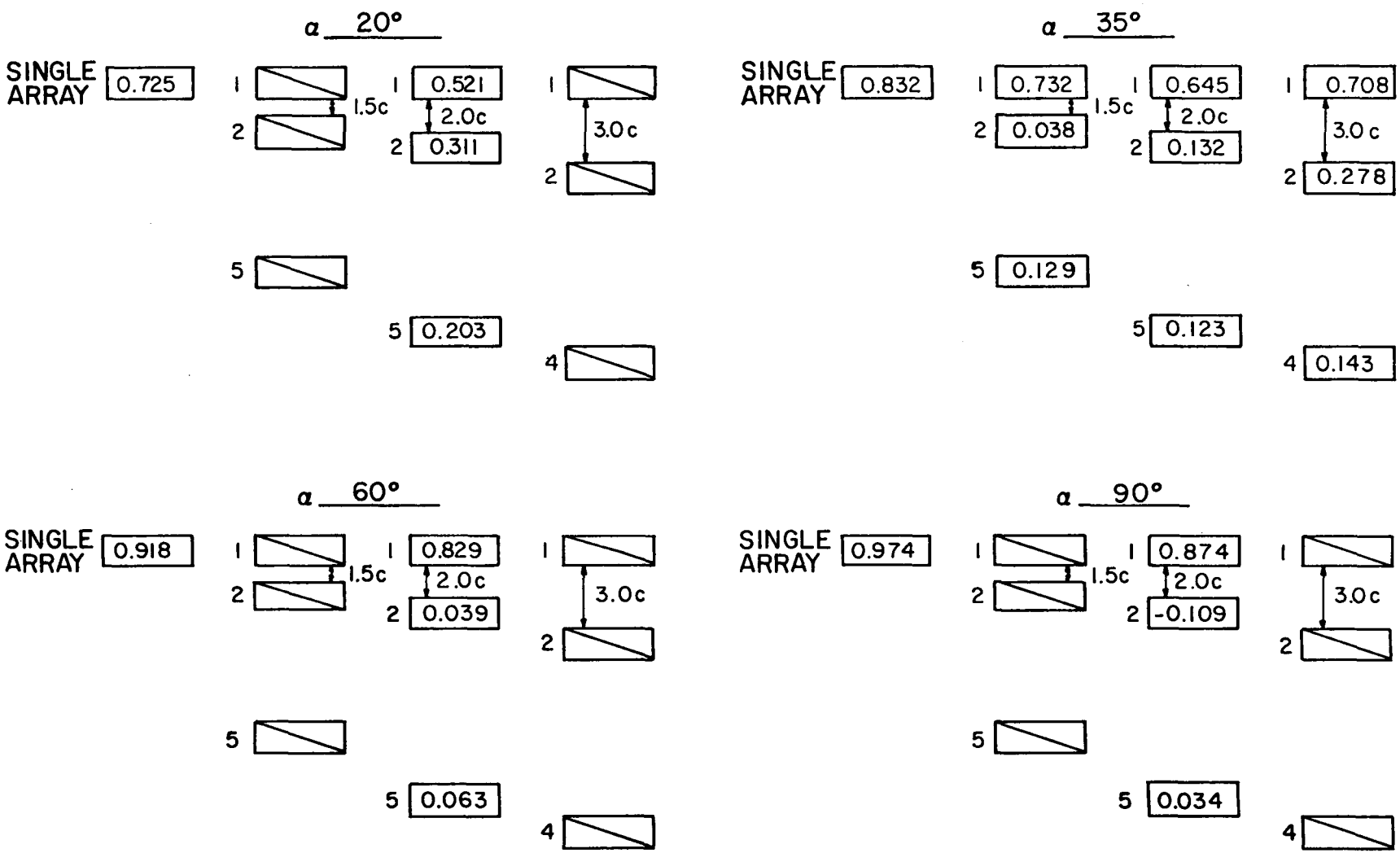

Figure 26. Normal Force Coefficients for an Array Field in Nonuniform Flow, No Fence, WD = 0°, H/c = 0.25, α = 20°, 35°, 60° and 90°

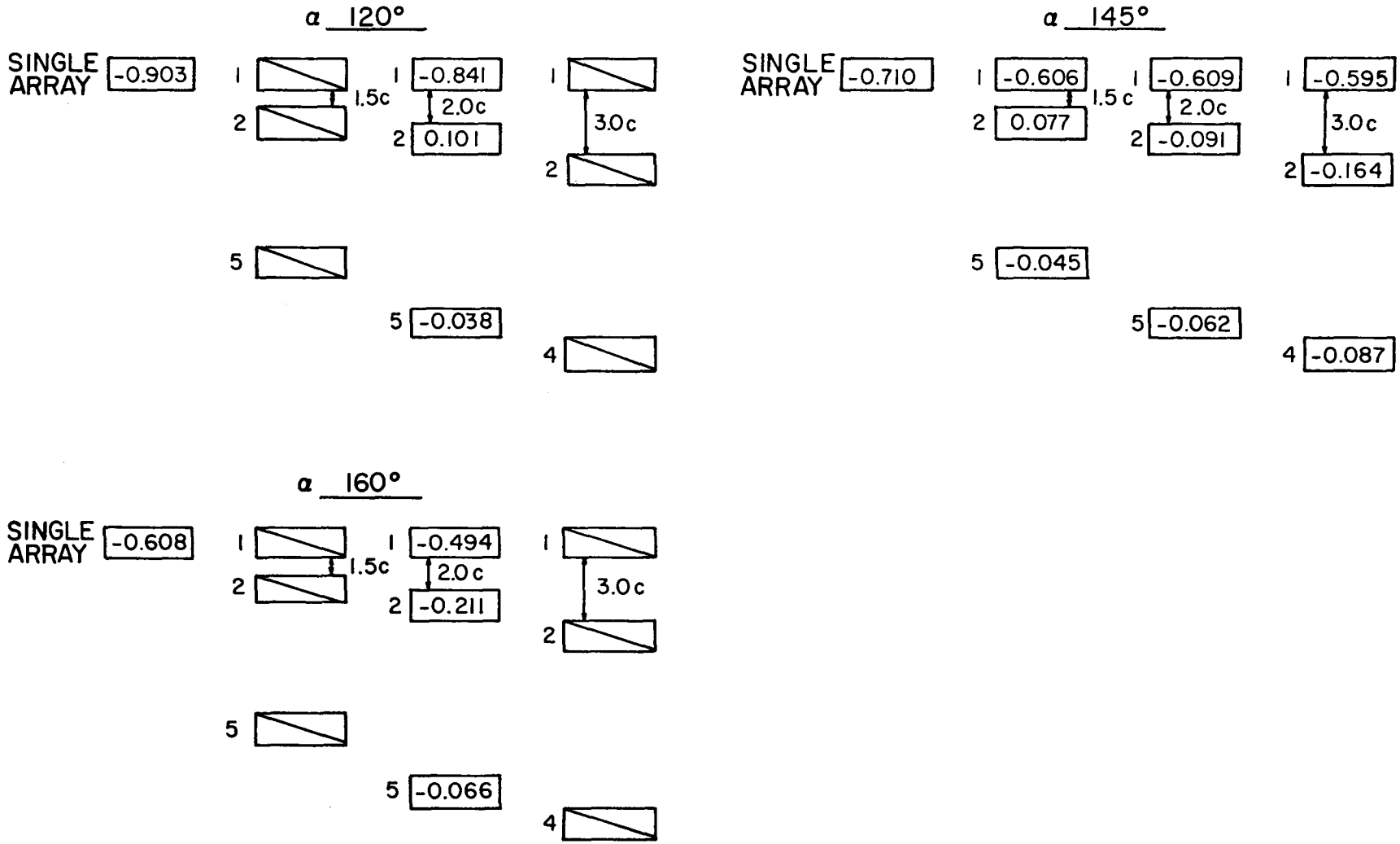

Figure 27. Normal Force Coefficients for an Array Field in Nonuniform Flow, No Fence, WD = 0°, H/c = 0.25, α = 120°, 145° and 160°

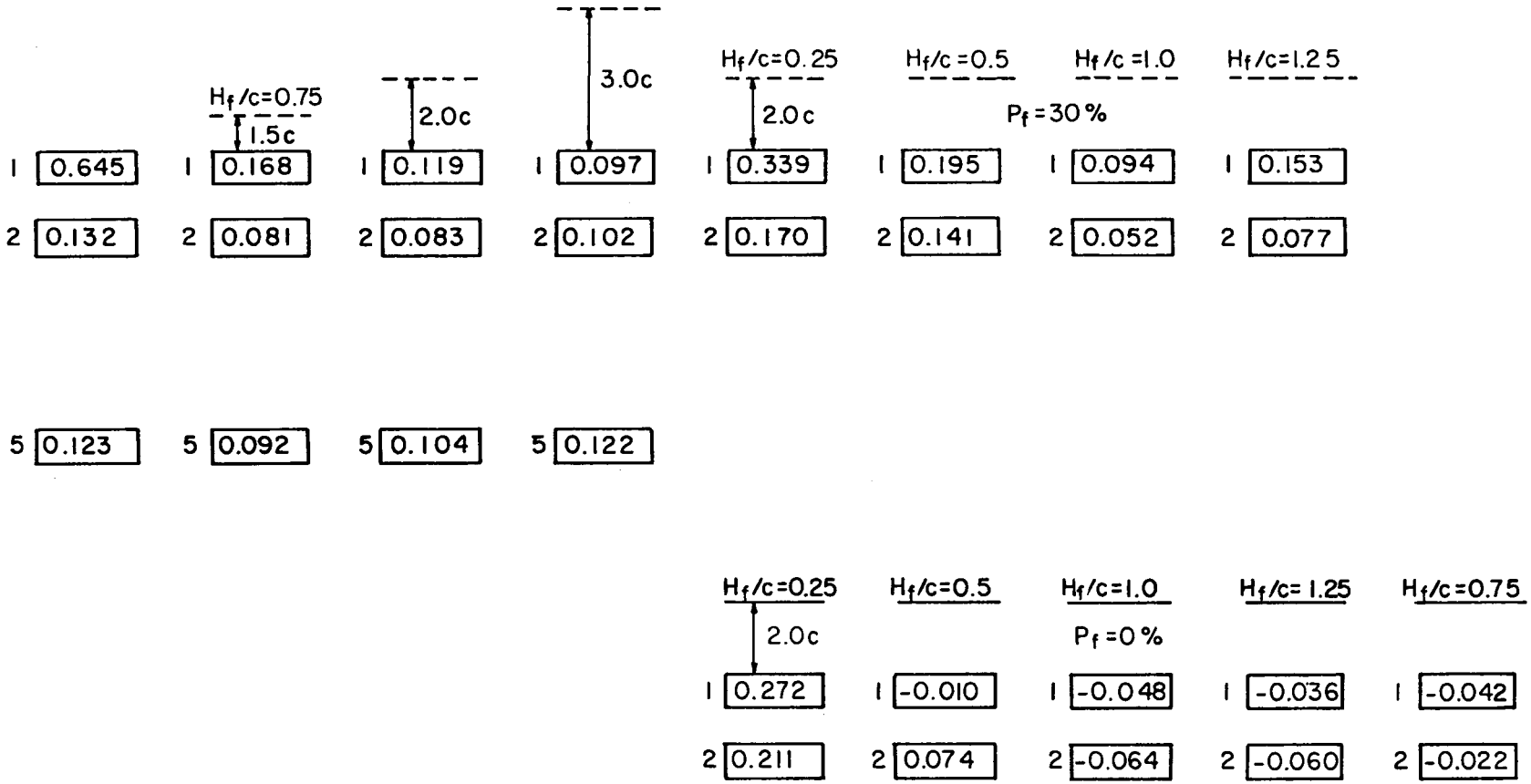

Figure 28a. Normal Force Coefficients for an Array Field with Various Fences, WD = 0°, x/c = 2.0, H/c = 0.25, α = 35°, Nonuniform Flow

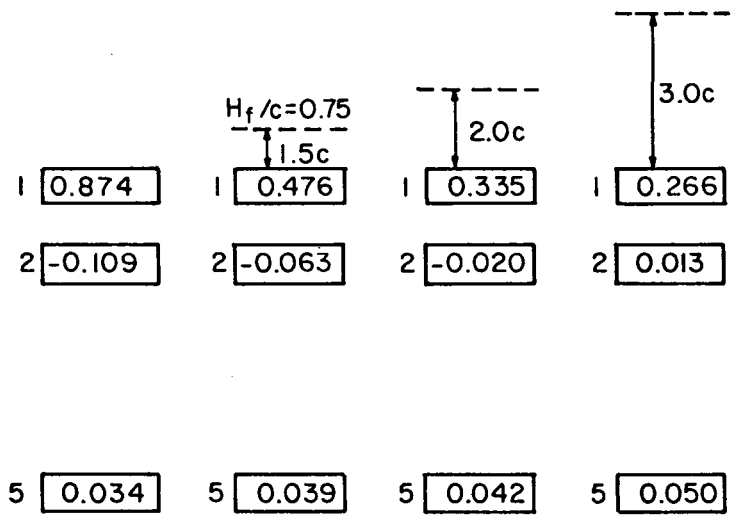

Figure 28b. Normal Force Coefficients for an Array Field with Various Fences, WD = 0°, x/c = 2.0, H/c = 0.25, α = 90°, Nonuniform Flow

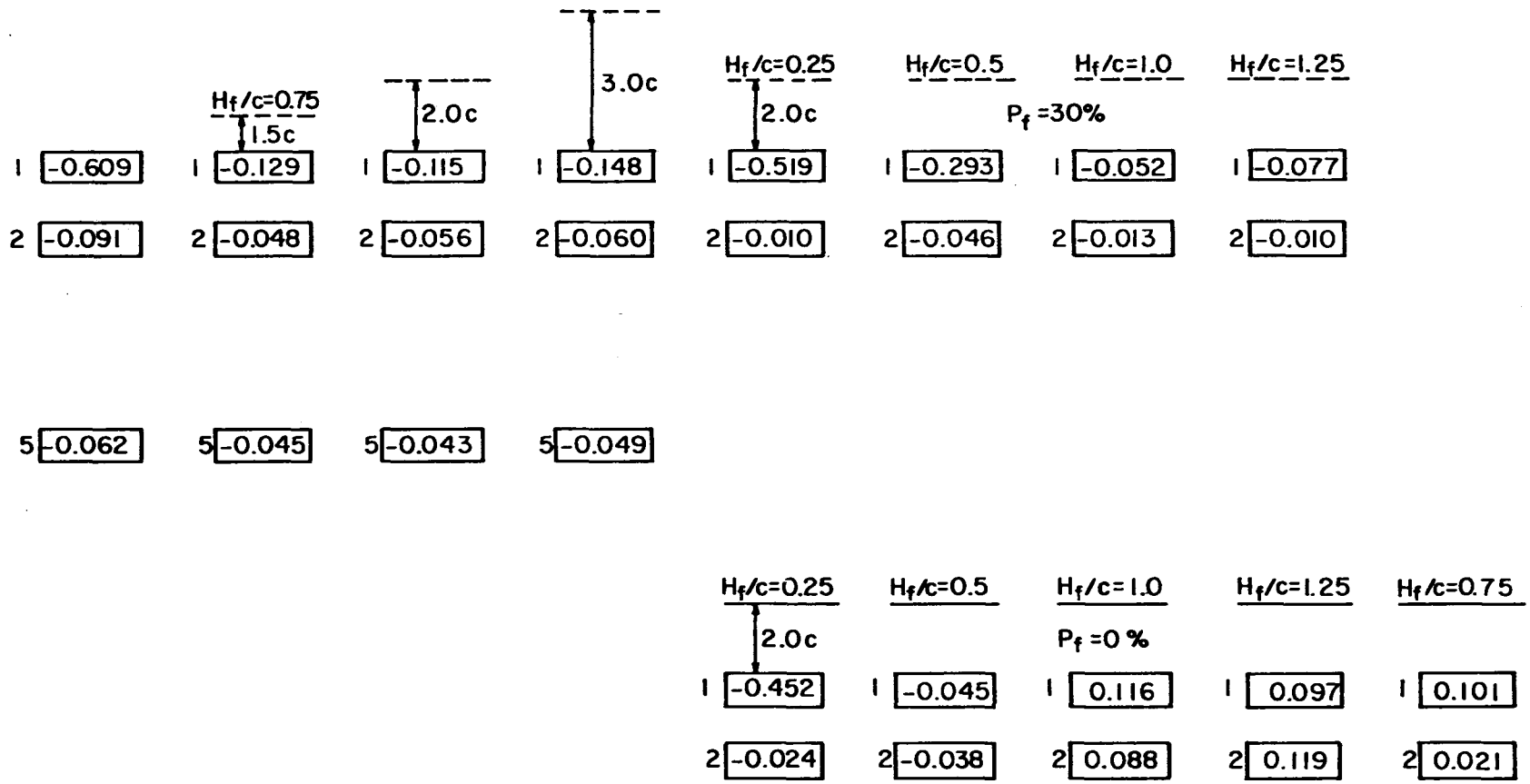

Figure 28c. Normal Force Coefficients for an Array Field with Various Fences, WD = 0°, x/c = 2.0, H/c = 0.25, α = 145°, Nonuniform Flow

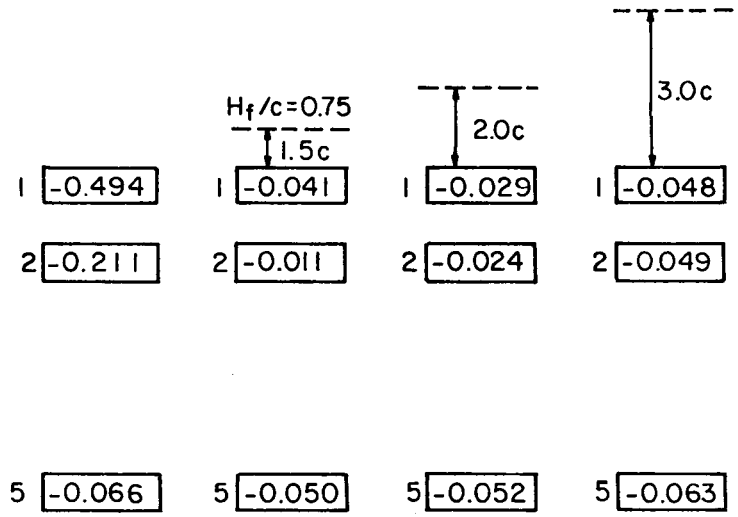

Figure 28d. Normal Force Coefficients for an Array Field with Various Fences, WD = 0°, x/c = 2.0, H/c = 0.25, α = 160°, Nonuniform Flow

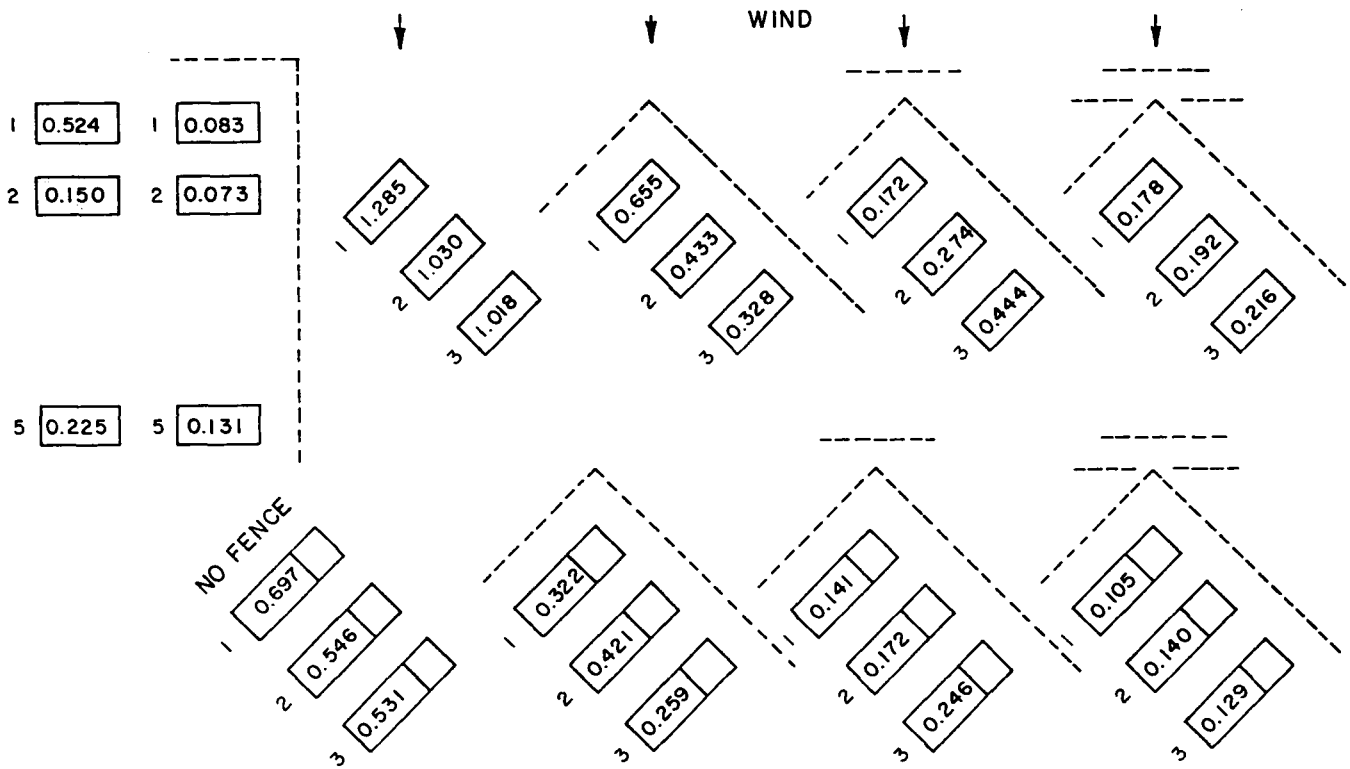

Figure 29a. Normal Force Coefficients for an Array Field, Edge and Corner Studies, x/c = 2.0, H/c = 0.25, α = 35°, Nonuniform Flow

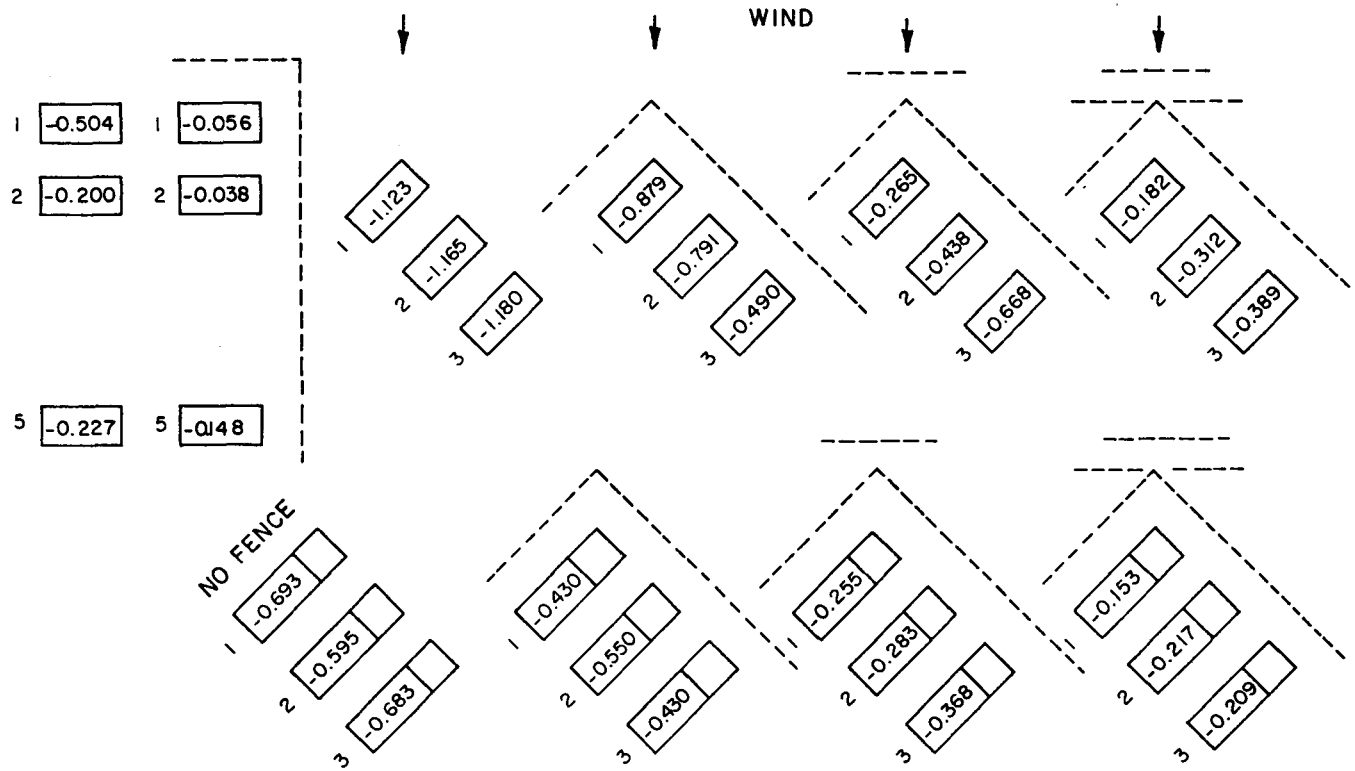

Figure 29b. Normal Force Coefficients for an Array Field, Edge and Corner Studies, x/c = 2.0, H/c = 0.25, α = 145°, Nonuniform Flow

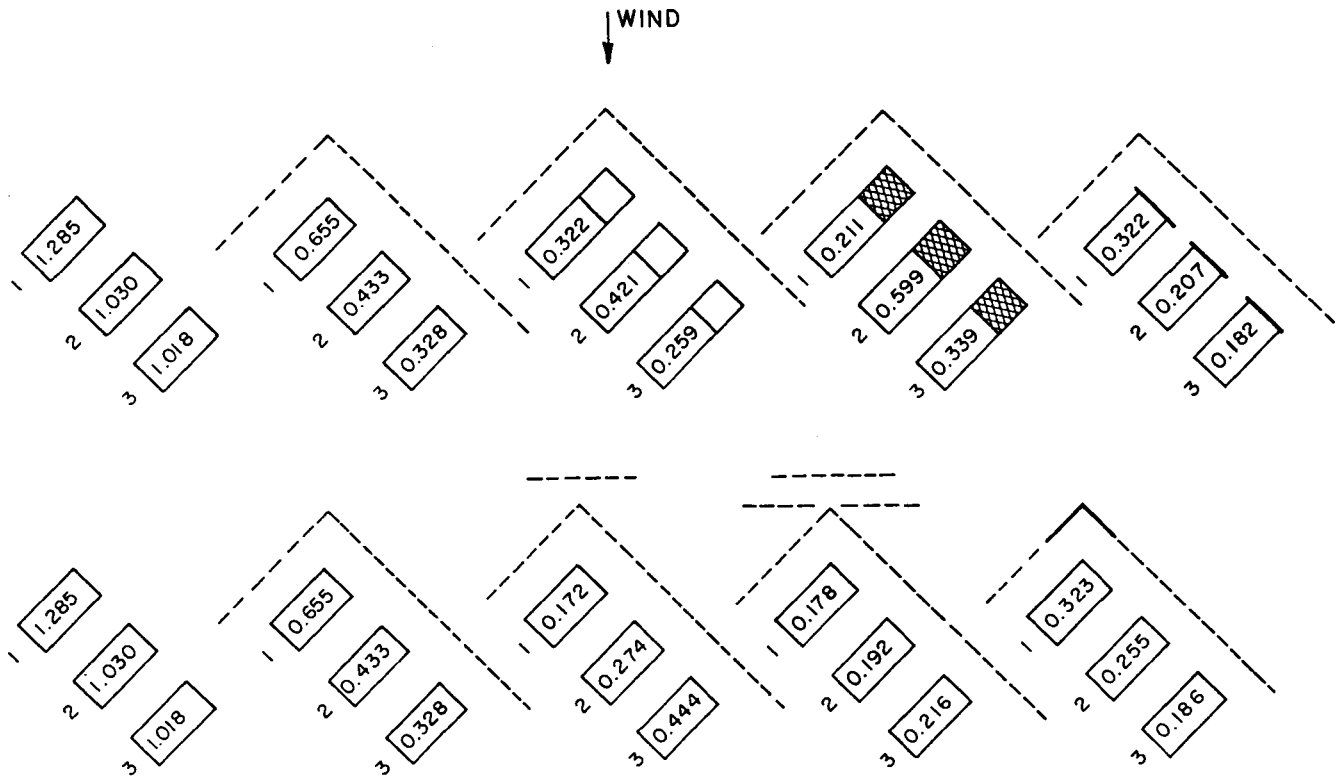

Figure 30a. Normal Force Coefficients for an Array Field, Corner Study with Various Fence and Model Configurations, x/c = 2.0, H/c = 0.25, α = 35°, Nonuniform Flow

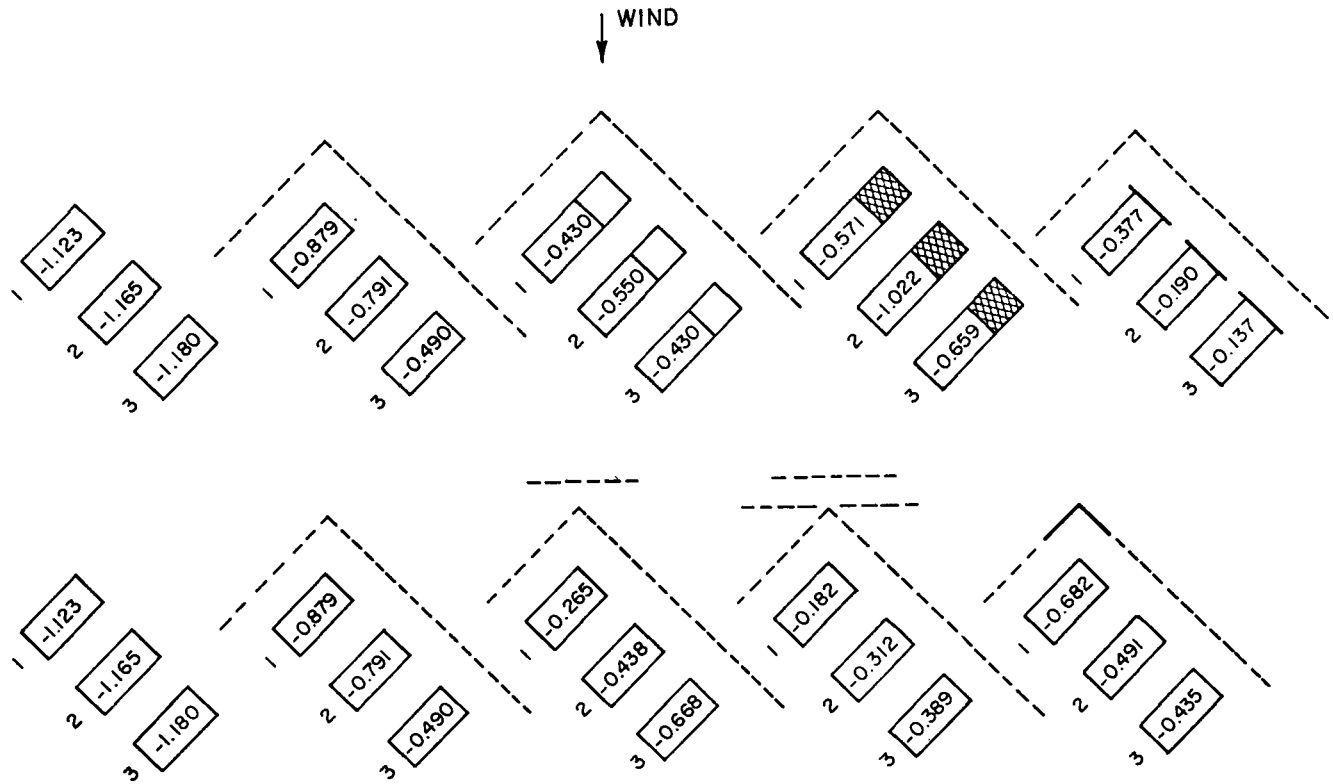

Figure 30b. Normal Force Coefficients for an Array Field, Corner Study with Various Fence and Model Configurations, x/c = 2.0, H/c = 0.25, α = 145°, Nonuniform flow

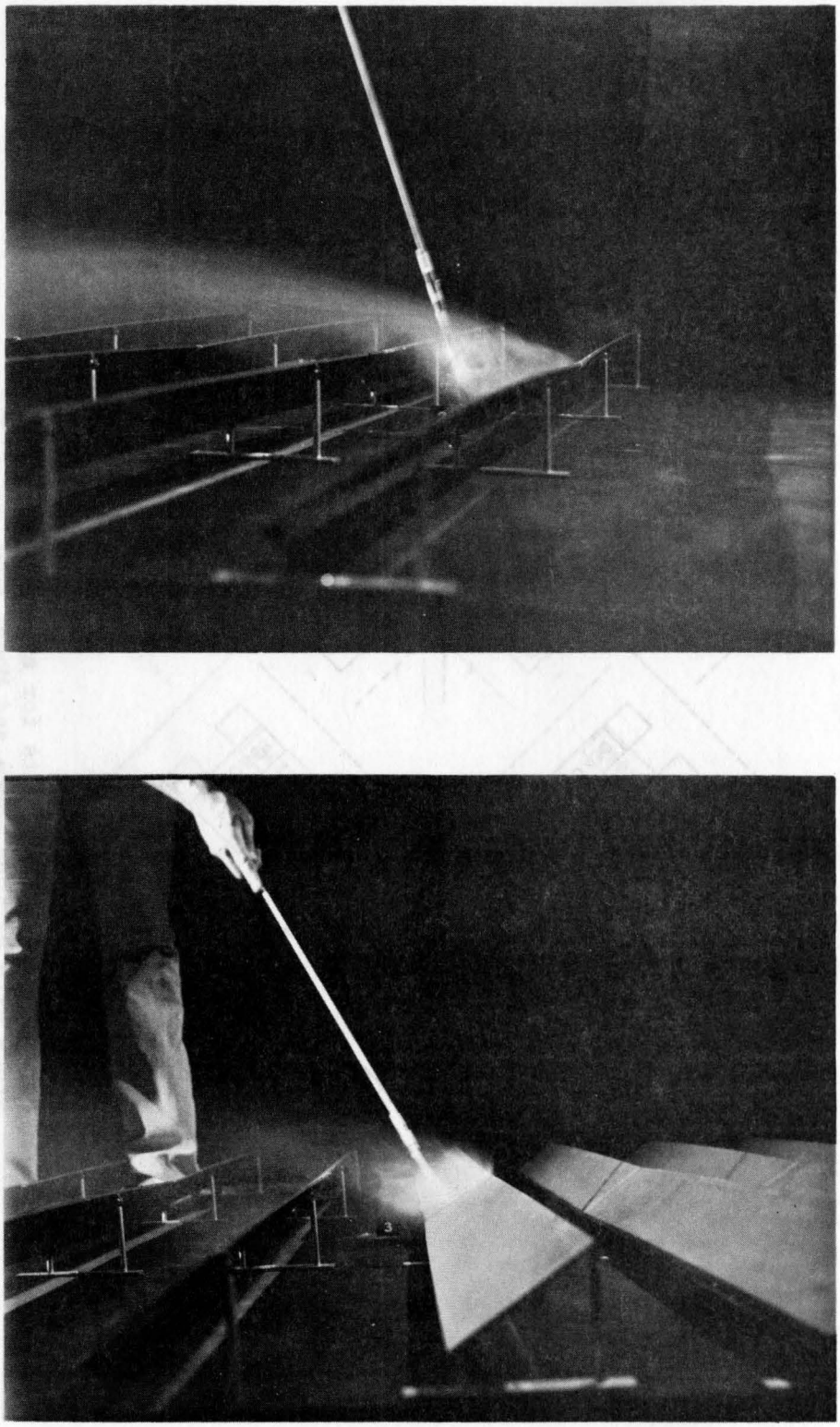

Figure 31a. Flow Visualization for an Array Field, WD = 0°

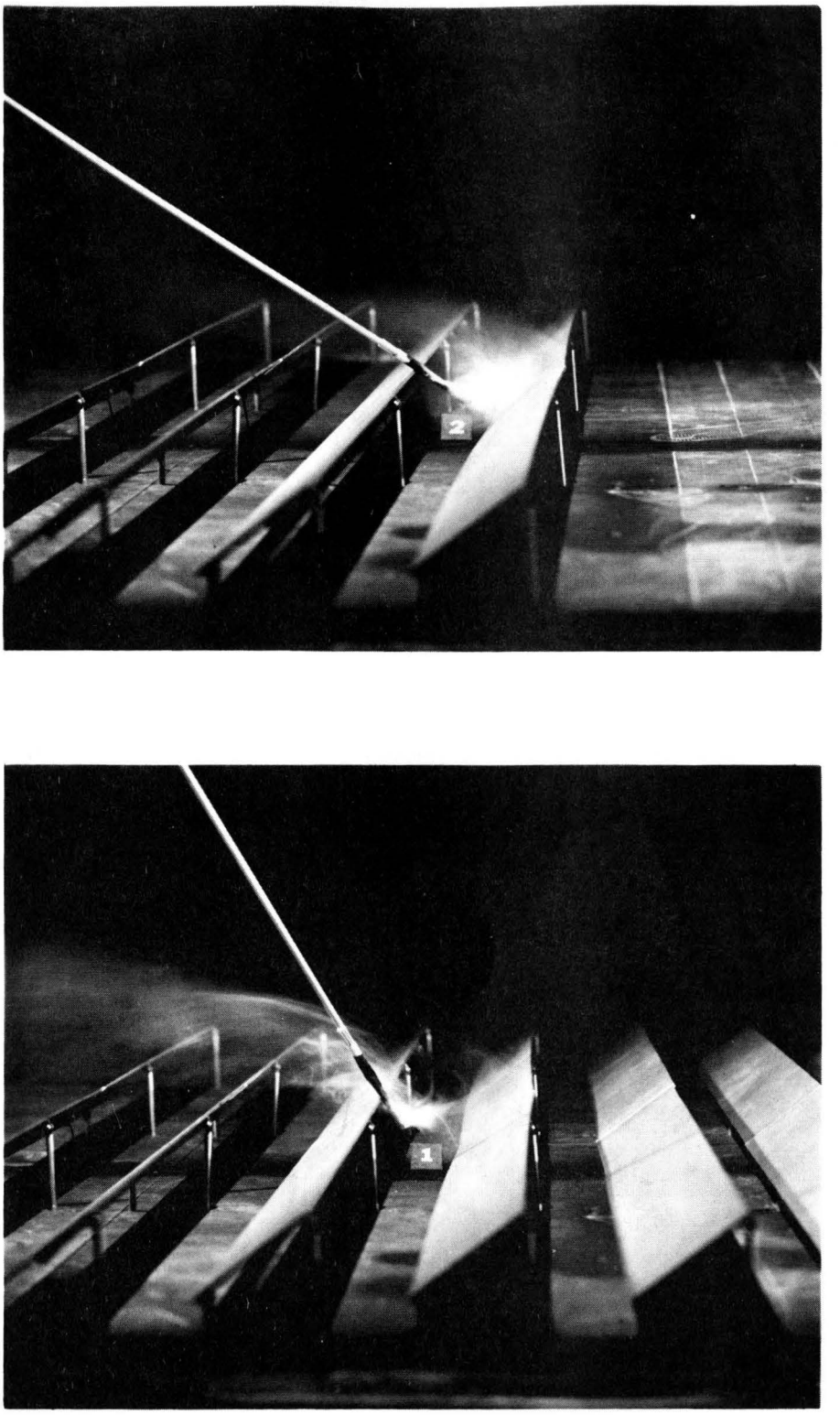

Figure 31b. Flow Visualization for an Array Field, WD = 0°

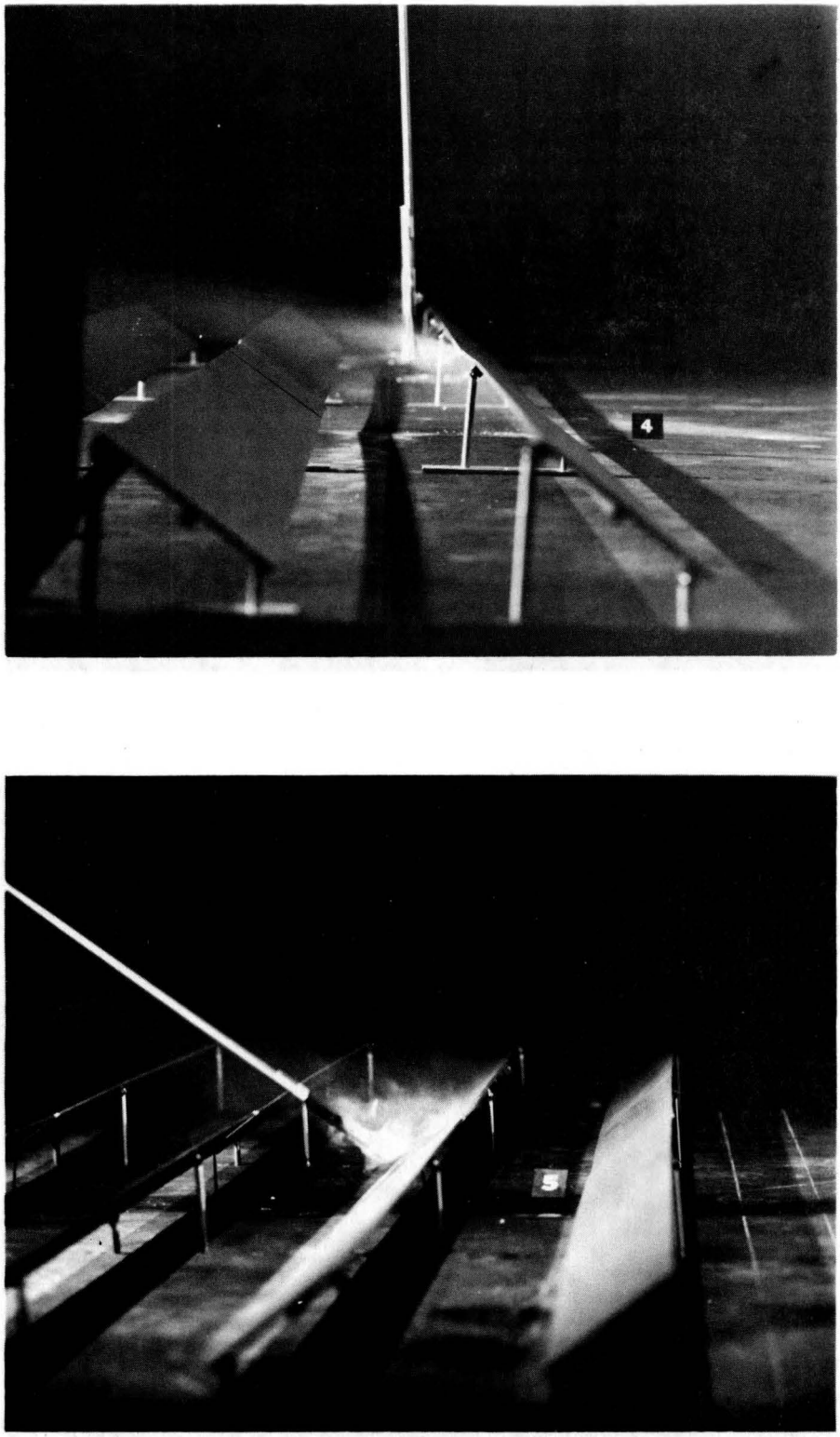

Figure 31c. Flow Visualization for an Array Field, WD = 0°

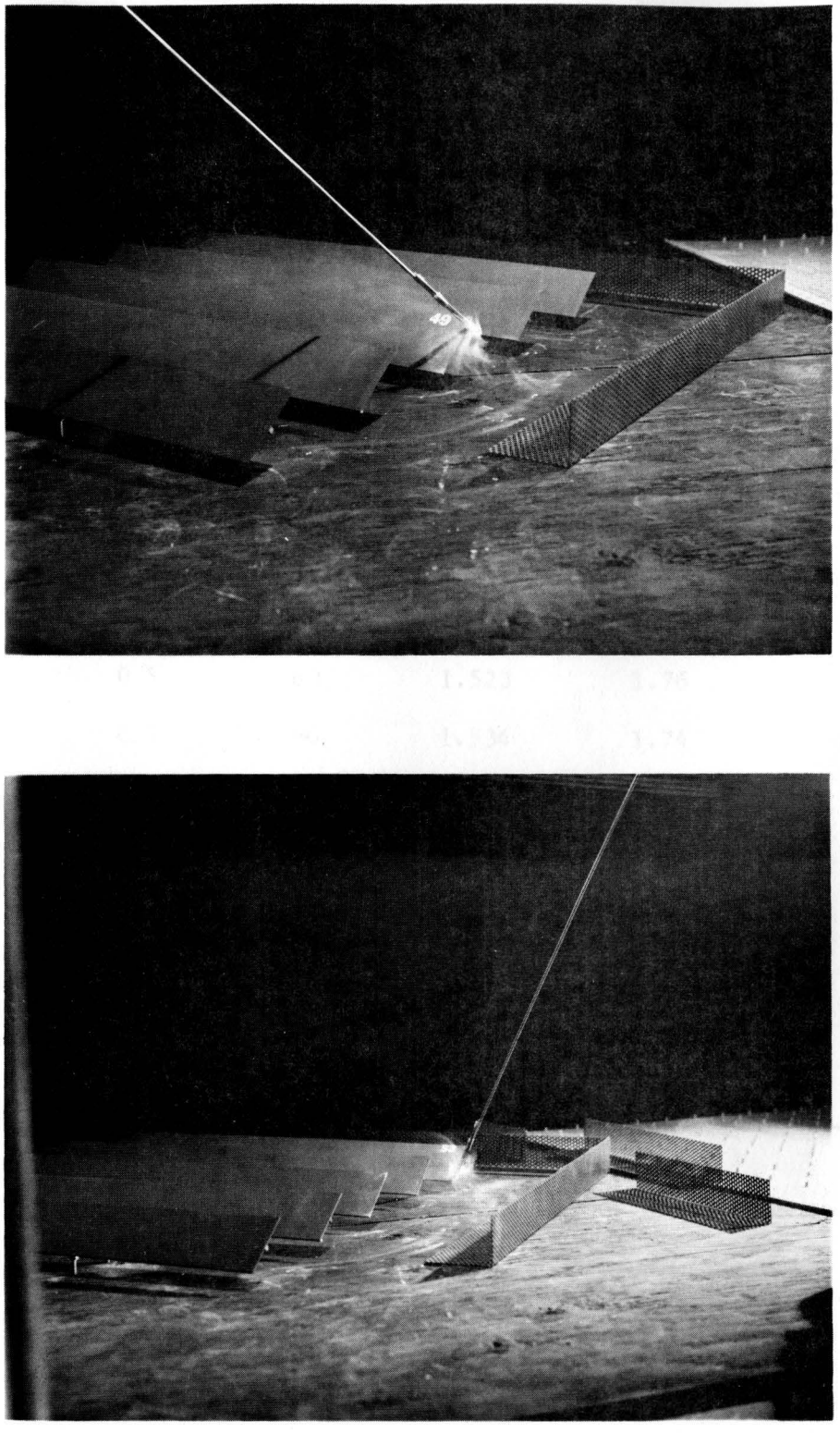

Figure 32. Flow Visualization for an Array Field, WD = 45°

TABLES

Table 1. Normal Force and Maximum Pressure Difference for a Single Array in Uniform Flow

File Name	H/c	α	C_N	$\Delta C_{p\ max}$	s_{max}/c
A02001	0.25	20	1.086	1.53	0.98
A03501	0.25	35	1.145	1.45	0.89
A06001	0.25	60	1.283	1.48	0.83
A09001	0.25	90	1.320	1.46	0.59
A12001	0.25	120	-1.320	-1.48	0.29
A14501	0.25	145	-1.024	-1.46	0.06
A16001	0.25	160	-0.885	-1.37	0.05
B02001	0.5	20	1.015	1.66	0.96
B06001	0.5	60	1.523	1.76	0.74
B09001	0.5	90	1.534	1.74	0.42
B12001	0.5	120	-1.440	-1.73	0.18
B16001	0.5	160	-0.936	-1.49	0.04
C02001	∞	20	1.133	1.79	0.97
C03501	∞	35	1.715	2.13	0.91
C06001	∞	60	2.228	2.48	0.71
C09001	∞	90	2.168	2.35	0.42

Table 2. Normal Force and Maximum Pressure Difference for an Array Field in Uniform Flow, x/c = 2.0

File Name	Array #	α	C_N	$\Delta C_{p\ max}$	s_{max}/c
E02001	1	20	0.717	1.06	0.96
E02101	2	20	0.210	0.82	0.73
E02201	5	20	0.267	0.91	0.86
E03501	1	35	1.006	1.24	0.91
E03601	2	35	0.383	0.75	0.26
E03701	5	35	0.100	0.20	0.45
E06001	1	60	1.220	1.39	0.84
E06101	2	60	-0.055	0.32	0.05
E06201	5	60	0.011	-0.04	0.46
E09001	1	90	1.400	1.56	0.58
E09101	2	90	-0.156	-0.28	0.59
E09201	5	90	-0.056	-0.07	0.42
E12001	1	120	-1.419	-1.60	0.27
E12101	2	120	0.277	0.38	0.28
E12201	5	120	-0.026	-0.10	0.92
E14501	1	145	-1.021	-1.38	0.04
E14601	2	145	-0.031	-0.11	0.74
E14701	5	145	-0.072	-0.10	0.83
E16001	1	160	-0.734	-1.10	0.05
E16101	2	160	-0.348	-0.48	0.05
E16201	5	160	-0.084	-0.10	0.59

Table 3. Normal Force and Maximum Pressure Difference for an Array Field in Uniform Flow, x/c = 1.5 and 3.0

File Name	x/c	Array #	α	C_N	$\Delta C_{p\ max}$	s_{max}/c
D03501	1.5	1	35	1.065	1.32	0.92
D03601	1.5	2	35	0.034	0.43	0.97
D03701	1.5	5	35	0.123	0.25	0.19
D14501	1.5	1	145	-1.076	-1.44	0.05
D14601	1.5	2	145	0.168	0.30	0.08
F03501	3.0	1	35	0.925	1.13	0.97
F03601	3.0	2	35	0.326	0.48	0.26
F03701	3.0	4	35	0.081	0.12	0.95
F14501	3.0	1	145	-0.937	-1.38	0.06
F14601	3.0	2	145	-0.063	-0.08	0.56
F14701	3.0	4	145	-0.116	-0.14	0.74

Table 4. Normal Force and Maximum Pressure Difference for a Single Array in Nonuniform Flow

File Name	H_f/c	α	C_N*	ΔC_p*$_{max}$	s_{max}/c
G02001	---	20	0.725	0.96	0.96
G03501	---	35	0.832	0.98	0.85
G06001	---	60	0.918	1.02	0.74
G09001	---	90	0.974	1.05	0.44
G12001	---	120	-0.903	-1.04	0.16
G14501	---	145	-0.710	-0.99	0.05
G16001	---	160	-0.608	-0.87	0.05
G01101	0.25	35	0.504	0.71	0.96
G01201	0.5	35	0.295	0.41	0.96
G01301	0.75	35	0.143	0.18	0.82
G01401	1.0	35	0.099	0.11	0.81
G01501	1.25	35	0.286	0.34	0.85
G02101	0.25	145	-0.577	-0.66	0.32
G02201	0.5	145	-0.309	-0.38	0.56
G02301	0.75	145	-0.120	-0.14	0.54
G02401	1.0	145	-0.066	-0.08	0.08
G02501	1.25	145	-0.196	-0.28	0.06

*referenced to 10 m on prototype

Table 5. Normal Force and Maximum Pressure Difference for an Array Field in Nonuniform Flow, x/c = 2.0

File Name	Array #	α	C_N*	$\Delta C_{p\,max}$*	s_{max}/c
I02001	1	20	0.521	0.73	0.95
I02101	2	20	0.311	0.38	0.74
I02201	5	20	0.203	0.31	0.90
I03501	1	35	0.645	0.76	0.91
I03601	2	35	0.132	0.29	0.20
I03701	5	35	0.123	0.15	0.74
I06001	1	60	0.829	0.90	0.75
I06101	2	60	0.039	0.34	0.06
I06201	5	60	0.063	0.08	0.83
I09001	1	90	0.874	0.97	0.28
I09101	2	90	-0.109	-0.20	0.57
I09201	5	90	0.034	0.08	0.96
I12001	1	120	-0.841	-0.94	0.17
I12101	2	120	0.101	0.17	0.42
I12201	5	120	-0.031	-0.08	0.92
I14501	1	145	-0.609	-0.83	0.05
I14601	2	145	-0.091	-0.11	0.13
I14701	5	145	-0.062	-0.08	0.78
I16001	1	160	-0.494	-0.71	0.05
I16101	2	160	-0.211	-0.32	0.05
I16201	5	160	-0.066	-0.08	0.59

*referenced to 10 m on prototype

Table 6. Normal Force and Maximum Pressure Difference for an Array Field in Nonuniform Flow, x/c = 1.5 and 3.0

File Name	x/c	Array #	α	C_N*	ΔC_p*$_{max}$	s_{max}/c
H03501	1.5	1	35	0.732	0.85	0.93
H03601	1.5	2	35	0.038	0.29	0.16
H03701	1.5	5	35	0.129	0.18	0.43
H14501	1.5	1	145	-0.606	-0.81	0.05
H14601	1.5	2	145	0.077	0.17	0.05
H14701	1.5	5	145	-0.045	-0.11	0.82
J03501	3.0	1	35	0.708	0.83	0.93
J03601	3.0	2	35	0.278	0.42	0.40
J03701	3.0	4	35	0.143	0.21	0.82
J14501	3.0	1	145	-0.595	-0.78	0.05
J14601	3.0	2	145	-0.164	-0.18	0.56
J14701	3.0	4	145	-0.087	-0.10	0.63

*referenced to 10 m on prototype

Table 7. Normal Force and Maximum Pressure Difference for an Array Field with a Fence, $H_f/c = 0.75$, $P_f = 30\%$, $x_f/c = 1.25$

File Name	Array #	α	C_N*	ΔC_p*max	s_{max}/c
K03501	1	35	0.168	0.20	0.82
K03601	2	35	0.081	0.10	0.53
K03701	5	35	0.092	0.14	0.90
K09001	1	90	0.476	0.53	0.84
K09101	2	90	-0.063	-0.13	0.46
K09201	5	90	0.039	0.08	0.86
K14501	1	145	-0.129	-0.15	0.17
K14601	2	145	-0.048	-0.06	0.76
K14701	5	145	-0.045	-0.07	0.77
K16001	1	160	-0.041	-0.06	0.11
K16101	2	160	-0.011	-0.03	0.82
K16201	5	160	-0.050	-0.07	0.61

*referenced to 10 m on prototype

Table 8. Normal Force and Maximum Pressure Difference for an Array Field with a Fence, $H_f/c = 0.75$, $P_f = 30\%$, $x_f/c = 2.5$

File Name	Array #	α	C_N*	ΔC_p*$_{max}$	s_{max}/c
L03501	1	35	0.119	0.13	0.58
L03601	2	35	0.083	0.11	0.83
L03701	5	35	0.104	0.13	0.84
L09001	1	90	0.335	0.38	0.83
L09101	2	90	-0.020	-0.04	0.44
L09201	5	90	0.042	0.08	0.92
L14501	1	145	-0.115	-0.13	0.73
L14601	2	145	-0.056	-0.08	0.77
L14701	5	145	-0.043	-0.08	0.85
L16001	1	160	-0.029	-0.06	0.12
L16101	2	160	-0.024	-0.03	0.58
L16201	5	160	-0.052	-0.08	0.58

*referenced to 10 m on prototype

Table 9. Normal Force and Maximum Pressure Difference for an Array Field with a Fence, $H_f/c = 0.75$, $P_f = 30\%$, $x_f/c = 5.0$

File Name	Array #	α	C_N*	ΔC_p*$_{max}$	s_{max}/c
M03501	1	35	0.097	0.13	0.83
M03601	2	35	0.102	0.14	0.84
M03701	5	35	0.122	0.17	0.95
M09001	1	90	0.266	0.34	0.82
M09101	2	90	0.013	0.03	0.24
M09201	5	90	0.050	0.08	0.96
M14501	1	145	-0.148	-0.27	0.44
M14601	2	145	-0.060	-0.10	0.77
M14701	5	145	-0.049	-0.08	0.76
M16001	1	160	-0.048	-0.06	0.28
M16101	2	160	-0.049	-0.07	0.60
M16201	5	160	-0.063	-0.08	0.55

*referenced to 10 m on prototype

Table 10. Normal Force and Maximum Pressure Difference for an Array Field with a Fence of Various Height and Porosity

File Name	P_f	H_f/c	Array #	α	C_N	$\Delta C_p^*{}_{max}$	s_{max}/c
N11101	30%	0.25	1	35	0.339	0.49	0.96
O11101	30%	0.25	2	35	0.170	0.22	0.41
N11201	30%	0.5	1	35	0.195	0.27	0.95
O11201	30%	0.5	2	35	0.141	0.20	0.89
N11401	30%	1.0	1	35	0.094	0.11	0.42
O11401	30%	1.0	2	35	0.052	0.08	0.43
N11501	30%	1.25	1	35	0.153	0.20	0.91
O11501	30%	1.25	2	35	0.077	0.13	0.42
N12101	30%	0.25	1	145	-0.519	-0.64	0.15
O12101	30%	0.25	2	145	-0.010	-0.06	0.76
N12201	30%	0.5	1	145	-0.293	-0.34	0.71
O12201	30%	0.5	2	145	-0.046	-0.10	0.78
N12401	30%	1.0	1	145	-0.052	-0.07	0.18
O12401	30%	1.0	2	145	-0.013	-0.06	0.74
N12501	30%	1.25	1	145	-0.077	-0.13	0.14
O12501	30%	1.25	2	145	-0.010	-0.03	0.74
NO1301	0%	0.75	1	35	-0.042	-0.06	0.26
OO1301	0%	0.75	2	35	-0.022	-0.04	0.26
NO2301	0%	0.75	1	145	0.101	0.15	0.41
OO2301	0%	0.75	2	145	0.021	0.06	0.26

*referenced to 10 m on prototype

Table 11. Normal Force and Maximum Pressure Difference for an Array Field, Edge Study

File Name	Fence	Array #	α	C_N*	ΔC_p*max	s_{max}/c
P03501	√	1	35	0.083	0.18	0.91
P03601	√	2	35	0.073	0.17	0.92
P03701	√	5	35	0.137	0.29	0.94
P14501	√	1	145	-0.056	-0.08	0.83
P14601	√	2	145	-0.038	-0.08	0.83
P14701	√	5	145	-0.148	-0.17	0.73
Q03501	---	1	35	0.524	0.78	0.95
Q03601	---	2	35	0.150	0.32	0.92
Q03701	---	5	35	0.225	0.46	0.95
Q14501	---	1	145	-0.504	-0.71	0.05
Q14601	---	2	145	-0.200	-0.34	0.06
Q14701	---	5	145	-0.227	-0.36	0.06

*referenced to 10 m on prototype

Table 12. Normal Force and Maximum Pressure Difference for an Array Field, No Fence, Corner Study

File Name	MC	Array #	α	C_N*	$\Delta C_p{}^*_{max}$	s_{max}/c
U03501	0	1	35	1.285	1.48	0.90
U03601	0	2	35	1.030	1.27	0.90
U03701	0	3	35	1.018	1.26	0.90
U14501	0	1	145	-1.123	-2.34	0.03
U14601	0	2	145	-1.165	-2.04	0.03
U14701	0	3	145	-1.180	-2.03	0.03
V03501	1	1	35	0.697	1.36	0.83
V03601	1	2	35	0.546	0.76	0.81
V03701	1	3	35	0.531	0.76	0.81
V14501	1	1	145	-0.693	-1.13	0.24
V14601	1	2	145	-0.595	-0.90	0.21
V14701	1	3	145	-0.638	-0.97	0.21

*referenced to 10 m on prototype

Table 13. Normal Force and Maximum Pressure Difference for an Array Field with Various Fences, Corner Study

File Name	FC	Array #	α	C_N*	ΔC_p*$_{max}$	s_{max}/c
R01101	1	1	35	0.655	1.93	0.96
S01101	1	2	35	0.433	1.09	0.96
T01101	1	3	35	0.328	0.62	0.96
R02101	1	1	145	0.879	-1.04	0.41
S02101	1	2	145	-0.791	-1.02	0.04
T02101	1	3	145	-0.490	-0.53	0.46
R01201	2	1	35	0.172	0.52	0.96
S01201	2	2	35	0.274	0.71	0.96
T01201	2	3	35	0.444	1.22	0.96
R02201	2	1	145	-0.265	-0.28	0.56
S02201	2	2	145	-0.438	-0.49	0.43
T02201	2	3	145	-0.668	-0.76	0.39
R01301	3	1	35	0.178	0.52	0.96
S01301	3	2	35	0.192	0.52	0.96
T01301	3	3	35	0.216	0.67	0.96
R02301	3	1	145	-0.182	-0.20	0.73
S02301	3	2	145	-0.312	-0.34	0.58
T02301	3	3	145	-0.389	-0.43	0.42

*referenced to 10 m on prototype

Table 14. Normal Force and Maximum Pressure Difference for an Array Field with Various Fences, MC = 1, Corner Study

File Name	FC	Array #	α	C_N*	ΔC_p*$_{max}$	s_{max}/c
R11101	1	1	35	0.322	0.77	0.96
S11101	1	2	35	0.421	0.78	0.96
T11101	1	3	35	0.259	0.34	0.84
R12101	1	1	145	-0.430	-0.50	0.43
S12101	1	2	145	-0.550	-0.64	0.40
T12101	1	3	145	-0.430	-0.50	0.27
R11201	2	1	35	0.141	0.27	0.97
S11201	2	2	35	0.172	0.31	0.97
T11201	2	3	35	0.246	0.50	0.97
R12201	2	1	145	-0.255	-0.29	0.43
S12201	2	2	145	-0.283	-0.34	0.38
T12201	2	3	145	-0.368	-0.43	0.29
R11301	3	1	35	0.105	0.20	0.96
S11301	3	2	35	0.140	0.27	0.96
T11301	3	3	35	0.129	0.22	0.96
R12301	3	1	145	-0.153	-0.17	0.43
S12301	3	2	145	-0.217	-0.27	0.43
T12301	3	3	145	-0.209	-0.25	0.43

*referenced to 10 m on prototype

Table 15. Normal Force and Maximum Pressure Difference for an Array Field with Various Models, FC = 1 and 4, Corner Study

File Name	MC	FC	α	Array #	C_N*	$\Delta C_p{}^*_{max}$	s_{max}/c
R21101	2	1	35	1	0.211	0.67	0.96
S21101	2	1	35	2	0.599	1.64	0.96
T21101	2	1	35	3	0.339	0.53	0.96
R22101	2	1	145	1	-0.571	-0.67	0.72
S22101	2	1	145	2	-1.022	-1.19	0.16
T22101	2	1	145	3	-0.659	-0.74	0.42
R31101	3	1	35	1	0.322	0.85	0.96
S31101	3	1	35	2	0.207	0.36	0.96
T31101	3	1	35	3	0.182	0.25	0.96
R32101	3	1	145	1	-0.377	-0.45	0.04
S32101	3	1	145	2	-0.190	-0.21	0.74
T32101	3	1	145	3	-0.137	-0.15	0.61
R01401	0	4	35	1	0.323	0.14	0.82
S01401	0	4	35	2	0.255	0.13	0.83
T01401	0	4	35	3	0.186	0.15	0.83
R02401	0	4	145	1	-0.682	-0.14	0.73
S02401	0	4	145	2	-0.491	-0.10	0.77
T02401	0	4	145	3	-0.435	-0.09	0.76

*referenced to 10 m on prototype

Table 16. Normal Force and Maximum Pressure Difference for an Array Field with a Fence, $H_f/c = 1.0$, $\alpha = 60°$ and $120°$

File Name	α	Array #	C_N*	ΔC_p*max	s_{max}/c
N23401	60	1	0.183	0.12	0.54
N24401	60	2	0.025	0.04	0.72
N25401	60	5	0.053	0.05	0.94
N33401	120	1	-0.165	-0.10	0.18
N34401	120	2	-0.015	-0.06	0.28
N35401	120	5	-0.048	-0.05	0.79

*referenced to 10 m on prototype

Table 17. Fence Configurations

FC	H_f/c	x_f/c	P_f	
1	0.75	2.5	30%	see Figure 22
2	0.75	2.5	30%	
3	0.75	2.5	30%	
4	0.75	2.5	30%	
5	0.75	1.25	30%	
6	0.75	5.0	30%	
7	0.25	2.5	30%	
8	0.5	2.5	30%	
9	1.0	2.5	30%	
10	1.25	2.5	30%	
11	0.25	2.5	0%	
12	0.5	2.5	0%	
13	0.75	2.5	0%	
14	1.0	2.5	0%	
15	1.25	2.5	0%	

Table 18. List of Test Configurations

File Name	Flow Profile		WD	Array		H/c	x	α	Array #	FC[1]	MC[2]
	Uniform	1/7 th		Single	Multiple						
A02001	✓		0	✓		0.25	-	20	-	-	0
A03501	✓		0	✓		0.25	-	35	-	-	0
A06001	✓		0	✓		0.25	-	60	-	-	0
A09001	✓		0	✓		0.25	-	90	-	-	0
A12001	✓		0	✓		0.25	-	120	-	-	0
A14501	✓		0	✓		0.25	-	145	-	-	0
A16001	✓		0	✓		0.25	-	160	-	-	0
B02001	✓		0	✓		0.5	-	20	-	-	0
B06001	✓		0	✓		0.5	-	60	-	-	0
B09001	✓		0	✓		0.5	-	90	-	-	0
B12001	✓		0	✓		0.5	-	120	-	-	0
B16001	✓		0	✓		0.5	-	160	-	-	0
C02001	✓		0	✓		∞	-	20	-	-	0
C03501	✓		0	✓		∞	-	35	-	-	0
C06001	✓		0	✓		∞	-	60	-	-	0
C09001	✓		0	✓		∞	-	90	-	-	0
D02001	✓		0		✓	0.25	1.5c	20	1	-	0
D02101	✓		0		✓	0.25	1.5c	20	2	-	0
D02201	✓		0		✓	0.25	1.5c	20	5	-	0
D03501	✓		0		✓	0.25	1.5c	35	1	-	0
D03601	✓		0		✓	0.25	1.5c	35	2	-	0
D03701	✓		0		✓	0.25	1.5c	35	5	-	0
D14501	✓		0		✓	0.25	1.5c	145	1	-	0
D14601	✓		0		✓	0.25	1.5c	145	2	-	0
D16001	✓		0		✓	0.25	1.5c	160	1	-	0
D16101	✓		0		✓	0.25	1.5c	160	2	-	0
E02001	✓		0		✓	0.25	2.0c	20	1	-	0
E02101	✓		0		✓	0.25	2.0c	20	2	-	0
E02201	✓		0		✓	0.25	2.0c	20	5	-	0
E03501	✓		0		✓	0.25	2.0c	35	1	-	0
E03601	✓		0		✓	0.25	2.0c	35	2	-	0
E03701	✓		0		✓	0.25	2.0c	35	5	-	0
E06001	✓		0		✓	0.25	2.0c	60	1	-	0
E06101	✓		0		✓	0.25	2.0c	60	2	-	0
E06201	✓		0		✓	0.25	2.0c	60	5	-	0
E09001	✓		0		✓	0.25	2.0c	90	1	-	0
E09101	✓		0		✓	0.25	2.0c	90	2	-	0
E09201	✓		0		✓	0.25	2.0c	90	5	-	0
E12001	✓		0		✓	0.25	2.0c	120	1	-	0
E12101	✓		0		✓	0.25	2.0c	120	2	-	0
E12201	✓		0		✓	0.25	2.0c	120	5	-	0
E14501	✓		0		✓	0.25	2.0c	145	1	-	0
E14601	✓		0		✓	0.25	2.0c	145	2	-	0
E14701	✓		0		✓	0.25	2.0c	145	5	-	0
E16001	✓		0		✓	0.25	2.0c	160	1	-	0
E16101	✓		0		✓	0.25	2.0c	160	2	-	0
E16201	✓		0		✓	0.25	2.0c	160	5	-	0
F03501	✓		0		✓	0.25	3.0c	35	1	-	0

[1] defined in Table 17

[2] defined in Figure 24

Table 18. (continued)

File Name	Flow Profile		WD	Array		H/c	x	α	Array #	FC	MC
	Uniform	1/7 th		Single	Multiple						
F03601	✓		0		✓	0.25	3.0c	35	2	-	0
F03701	✓		0		✓	0.25	3.0c	35	4	-	0
F06001	✓		0		✓	0.25	3.0c	60	1	-	0
F06101	✓		0		✓	0.25	3.0c	60	2	-	0
F06201	✓		0		✓	0.25	3.0c	60	4	-	0
F12001	✓		0		✓	0.25	3.0c	120	1	-	0
F12101	✓		0		✓	0.25	3.0c	120	2	-	0
F12201	✓		0		✓	0.25	3.0c	120	4	-	0
F14501	✓		0		✓	0.25	3.0c	145	1	-	0
F14601	✓		0		✓	0.25	3.0c	145	2	-	0
F14701	✓		0		✓	0.25	3.0c	145	4	-	0
G02001		✓	0	✓		0.25	-	20	-	-	0
G03501		✓	0	✓		0.25	-	35	-	-	0
G06001		✓	0	✓		0.25	-	60	-	-	0
G09001		✓	0	✓		0.25	-	90	-	-	0
G12001		✓	0	✓		0.25	-	120	-	-	0
G14501		✓	0	✓		0.25	-	145	-	-	0
G16001		✓	0	✓		0.25	-	160	-	-	0
G01101		✓	0	✓		0.25	-	35	-	7	0
G01201		✓	0	✓		0.25	-	35	-	8	0
G01301		✓	0	✓		0.25	-	35	-	1	0
G01401		✓	0	✓		0.25	-	35	-	9	0
G01501		✓	0	✓		0.25	-	35	-	10	0
G02101		✓	0	✓		0.25	-	145	-	7	0
G02201		✓	0	✓		0.25	-	145	-	8	0
G02301		✓	0	✓		0.25	-	145	-	1	0
G02401		✓	0	✓		0.25	-	145	-	9	0
G02501		✓	0	✓		0.25	-	145	-	10	0
H02001		✓	0		✓	0.25	1.5c	20	1	-	0
H02101		✓	0		✓	0.25	1.5c	20	2	-	0
H02201		✓	0		✓	0.25	1.5c	20	5	-	0
H03501		✓	0		✓	0.25	1.5c	35	1	-	0
H03601		✓	0		✓	0.25	1.5c	35	2	-	0
H03701		✓	0		✓	0.25	1.5c	35	5	-	0
H14501		✓	0		✓	0.25	1.5c	145	1	-	0
H14601		✓	0		✓	0.25	1.5c	145	2	-	0
H14701		✓	0		✓	0.25	1.5c	145	5	-	0
H16001		✓	0		✓	0.25	1.5c	160	1	-	0
H16101		✓	0		✓	0.25	1.5c	160	2	-	0
H16201		✓	0		✓	0.25	1.5c	160	5	-	0
I02001		✓	0		✓	0.25	2.0c	20	1	-	0
I02101		✓	0		✓	0.25	2.0c	20	2	-	0
I02201		✓	0		✓	0.25	2.0c	20	5	-	0
I03501		✓	0		✓	0.25	2.0c	35	1	-	0
I03601		✓	0		✓	0.25	2.0c	35	2	-	0
I03701		✓	0		✓	0.25	2.0c	35	5	-	0
I06001		✓	0		✓	0.25	2.0c	60	1	-	0
I06101		✓	0		✓	0.25	2.0c	60	2	-	0

Table 18. (continued)

File Name	Flow Profile		WD	Array		H/c	x	α	Array #	FC	MC
	Uniform	1/7 th		Single	Multiple						
I06201		✓	0		✓	0.25	2.0c	60	5	-	0
I09001		✓	0		✓	0.25	2.0c	90	1	-	0
I09101		✓	0		✓	0.25	2.0c	90	2	-	0
I09201		✓	0		✓	0.25	2.0c	90	5	-	0
I12001		✓	0		✓	0.25	2.0c	120	1	-	0
I12101		✓	0		✓	0.25	2.0c	120	2	-	0
I12201		✓	0		✓	0.25	2.0c	120	5	-	0
I14501		✓	0		✓	0.25	2.0c	145	1	-	0
I14601		✓	0		✓	0.25	2.0c	145	2	-	0
I14701		✓	0		✓	0.25	2.0c	145	5	-	0
I16001		✓	0		✓	0.25	2.0c	160	1	-	0
I16101		✓	0		✓	0.25	2.0c	160	2	-	0
I16201		✓	0		✓	0.25	2.0c	160	5	-	0
J03501		✓	0		✓	0.25	3.0c	35	1	-	0
J03601		✓	0		✓	0.25	3.0c	35	2	-	0
J03701		✓	0		✓	0.25	3.0c	35	4	-	0
J06001		✓	0		✓	0.25	3.0c	60	1	-	0
J06101		✓	0		✓	0.25	3.0c	60	2	-	0
J06201		✓	0		✓	0.25	3.0c	60	4	-	0
J12001		✓	0		✓	0.25	3.0c	120	1	-	0
J12101		✓	0		✓	0.25	3.0c	120	2	-	0
J12201		✓	0		✓	0.25	3.0c	120	4	-	0
J14501		✓	0		✓	0.25	3.0c	145	1	-	0
J14601		✓	0		✓	0.25	3.0c	145	2	-	0
J14701		✓	0		✓	0.25	3.0c	145	4	-	0
K03501		✓	0		✓	0.25	2.0c	35	1	5	0
K03601		✓	0		✓	0.25	2.0c	35	2	5	0
K03701		✓	0		✓	0.25	2.0c	35	5	5	0
K09001		✓	0		✓	0.25	2.0c	90	1	5	0
K09101		✓	0		✓	0.25	2.0c	90	2	5	0
K09201		✓	0		✓	0.25	2.0c	90	5	5	0
K14501		✓	0		✓	0.25	2.0c	145	1	5	0
K14601		✓	0		✓	0.25	2.0c	145	2	5	0
K14701		✓	0		✓	0.25	2.0c	145	5	5	0
K16001		✓	0		✓	0.25	2.0c	160	1	5	0
K16101		✓	0		✓	0.25	2.0c	160	2	5	0
K16201		✓	0		✓	0.25	2.0c	160	5	5	0
L03501		✓	0		✓	0.25	2.0c	35	1	1	0
L03601		✓	0		✓	0.25	2.0c	35	2	1	0
L03701		✓	0		✓	0.25	2.0c	35	5	1	0
L09001		✓	0		✓	0.25	2.0c	90	1	1	0
L09101		✓	0		✓	0.25	2.0c	90	2	1	0
L09201		✓	0		✓	0.25	2.0c	90	5	1	0
L14501		✓	0		✓	0.25	2.0c	145	1	1	0
L14601		✓	0		✓	0.25	2.0c	145	2	1	0
L14701		✓	0		✓	0.25	2.0c	145	5	1	0
L16001		✓	0		✓	0.25	2.0c	160	1	1	0
L16101		✓	0		✓	0.25	2.0c	160	2	1	0

Table 18. (continued)

File Name	Flow Profile		WD	Array		H/c	x	α	Array #	FC	MC
	Uniform	1/7 th		Single	Multiple						
L16201		✓	0		✓	0.25	2.0c	160	5	1	0
M03501		✓	0		✓	0.25	2.0c	35	1	6	0
M03601		✓	0		✓	0.25	2.0c	35	2	6	0
M03701		✓	0		✓	0.25	2.0c	35	5	6	0
M09001		✓	0		✓	0.25	2.0c	90	1	6	0
M09101		✓	0		✓	0.25	2.0c	90	2	6	0
M09201		✓	0		✓	0.25	2.0c	90	5	6	0
M14501		✓	0		✓	0.25	2.0c	145	1	6	0
M14601		✓	0		✓	0.25	2.0c	145	2	6	0
M14701		✓	0		✓	0.25	2.0c	145	5	6	0
M16001		✓	0		✓	0.25	2.0c	160	1	6	0
M16101		✓	0		✓	0.25	2.0c	160	2	6	0
M16201		✓	0		✓	0.25	2.0c	160	5	6	0
N01101		✓	0		✓	0.25	2.0c	35	1	11	0
N01201		✓	0		✓	0.25	2.0c	35	1	12	0
N01301		✓	0		✓	0.25	2.0c	35	1	13	0
N01401		✓	0		✓	0.25	2.0c	35	1	14	0
N01501		✓	0		✓	0.25	2.0c	35	1	15	0
N02101		✓	0		✓	0.25	2.0c	145	1	11	0
N02201		✓	0		✓	0.25	2.0c	145	1	12	0
N02301		✓	0		✓	0.25	2.0c	145	1	13	0
N02401		✓	0		✓	0.25	2.0c	145	1	14	0
N02501		✓	0		✓	0.25	2.0c	145	1	15	0
N11101		✓	0		✓	0.25	2.0c	35	1	7	0
N11201		✓	0		✓	0.25	2.0c	35	1	8	0
N11401		✓	0		✓	0.25	2.0c	35	1	9	0
N11501		✓	0		✓	0.25	2.0c	35	1	10	0
N12101		✓	0		✓	0.25	2.0c	145	1	7	0
N12201		✓	0		✓	0.25	2.0c	145	1	8	0
N12401		✓	0		✓	0.25	2.0c	145	1	9	0
N12501		✓	0		✓	0.25	2.0c	145	1	10	0
N23401		✓	0		✓	0.25	2.0c	60	1	9	0
N24401		✓	0		✓	0.25	2.0c	60	2	9	0
N25401		✓	0		✓	0.25	2.0c	60	5	9	0
N33401		✓	0		✓	0.25	2.0c	120	1	9	0
N34401		✓	0		✓	0.25	2.0c	120	2	9	0
N35401		✓	0		✓	0.25	2.0c	120	5	9	0
O01101		✓	0		✓	0.25	2.0c	35	2	11	0
O01201		✓	0		✓	0.25	2.0c	35	2	12	0
O01301		✓	0		✓	0.25	2.0c	35	2	13	0
O01401		✓	0		✓	0.25	2.0c	35	2	14	0
O01501		✓	0		✓	0.25	2.0c	35	2	15	0
O02101		✓	0		✓	0.25	2.0c	145	2	11	0
O02201		✓	0		✓	0.25	2.0c	145	2	12	0
O02301		✓	0		✓	0.25	2.0c	145	2	13	0
O02401		✓	0		✓	0.25	2.0c	145	2	14	0
O02501		✓	0		✓	0.25	2.0c	145	2	15	0
O11101		✓	0		✓	0.25	2.0c	35	2	7	0

Table 18. (continued)

File Name	Flow Profile		WD	Array		H/c	x	α	Array #	FC	MC
	Uniform	1/7 th		Single	Multiple						
O11201		✓	0		✓	0.25	2.0c	35	2	8	0
O11401		✓	0		✓	0.25	2.0c	35	2	9	0
O11501		✓	0		✓	0.25	2.0c	35	2	10	0
O12101		✓	0		✓	0.25	2.0c	145	2	7	0
O12201		✓	0		✓	0.25	2.0c	145	2	8	0
O12401		✓	0		✓	0.25	2.0c	145	2	9	0
O12501		✓	0		✓	0.25	2.0c	145	2	10	0
P03501		✓	0		✓ (edge)	0.25	2.0c	35	1	1	0
P03601		✓	0		✓ (edge)	0.25	2.0c	35	2	1	0
P03701		✓	0		✓ (edge)	0.25	2.0c	35	5	1	0
P14501		✓	0		✓ (edge)	0.25	2.0c	145	1	1	0
P14601		✓	0		✓ (edge)	0.25	2.0c	145	2	1	0
P14701		✓	0		✓ (edge)	0.25	2.0c	145	5	1	0
Q03501		✓	0		✓ (edge)	0.25	2.0c	35	1	-	0
Q03601		✓	0		✓ (edge)	0.25	2.0c	35	2	-	0
Q03701		✓	0		✓ (edge)	0.25	2.0c	35	5	-	0
Q14501		✓	0		✓ (edge)	0.25	2.0c	145	1	-	0
Q14601		✓	0		✓ (edge)	0.25	2.0c	145	2	-	0
Q14701		✓	0		✓ (edge)	0.25	2.0c	145	5	-	0
R01101		✓	45		✓	0.25	2.0c	35	1	1	0
R02101		✓	45		✓	0.25	2.0c	145	1	1	0
R01201		✓	45		✓	0.25	2.0c	35	1	2	0
R02201		✓	45		✓	0.25	2.0c	145	1	2	0
R01301		✓	45		✓	0.25	2.0c	35	1	3	0
R02301		✓	45		✓	0.25	2.0c	145	1	3	0
R01401		✓	45		✓	0.25	2.0c	35	1	4	0
R02401		✓	45		✓	0.25	2.0c	145	1	4	0
R11101		✓	45		✓	0.25	2.0c	35	1	1	1
R12101		✓	45		✓	0.25	2.0c	145	1	1	1
R11201		✓	45		✓	0.25	2.0c	35	1	2	1
R12201		✓	45		✓	0.25	2.0c	145	1	2	1
R11301		✓	45		✓	0.25	2.0c	35	1	3	1
R12301		✓	45		✓	0.25	2.0c	145	1	3	1
R21101		✓	45		✓	0.25	2.0c	35	1	1	2
R22101		✓	45		✓	0.25	2.0c	145	1	1	2
R31101		✓	45		✓	0.25	2.0c	35	1	1	3
R32101		✓	45		✓	0.25	2.0c	145	1	1	3
S01101		✓	45		✓	0.25	2.0c	35	2	1	0
S02101		✓	45		✓	0.25	2.0c	145	2	1	0
S01201		✓	45		✓	0.25	2.0c	35	2	2	0
S02201		✓	45		✓	0.25	2.0c	145	2	2	0
S01301		✓	45		✓	0.25	2.0c	35	2	3	0
S02301		✓	45		✓	0.25	2.0c	145	2	3	0
S01401		✓	45		✓	0.25	2.0c	35	2	4	0
S02401		✓	45		✓	0.25	2.0c	145	2	4	0
S11101		✓	45		✓	0.25	2.0c	35	2	1	1
S12101		✓	45		✓	0.25	2.0c	145	2	1	1
S11201		✓	45		✓	0.25	2.0c	35	2	2	1

Table 18. (continued)

File Name	Flow Profile		WD	Array		H/c	x	α	Array #	FC	MC
	Uniform	1/7 th		Single	Multiple						
S12201		✓	45		✓	0.25	2.0c	145	2	2	1
S11301		✓	45		✓	0.25	2.0c	35	2	3	1
S12301		✓	45		✓	0.25	2.0c	145	2	3	1
S21101		✓	45		✓	0.25	2.0c	35	2	1	2
S22101		✓	45		✓	0.25	2.0c	145	2	1	2
S31101		✓	45		✓	0.25	2.0c	35	2	1	3
S32101		✓	45		✓	0.25	2.0c	145	2	1	3
T01101		✓	45		✓	0.25	2.0c	35	3	1	0
T02101		✓	45		✓	0.25	2.0c	145	3	1	0
T01201		✓	45		✓	0.25	2.0c	35	3	2	0
T02201		✓	45		✓	0.25	2.0c	145	3	2	0
T01301		✓	45		✓	0.25	2.0c	35	3	3	0
T02301		✓	45		✓	0.25	2.0c	145	3	3	0
T01401		✓	45		✓	0.25	2.0c	35	3	4	0
T02401		✓	45		✓	0.25	2.0c	145	3	4	0
T11101		✓	45		✓	0.25	2.0c	35	3	1	1
T12101		✓	45		✓	0.25	2.0c	145	3	1	1
T11201		✓	45		✓	0.25	2.0c	35	3	2	1
T12201		✓	45		✓	0.25	2.0c	145	3	2	1
T11301		✓	45		✓	0.25	2.0c	35	3	3	1
T12301		✓	45		✓	0.25	2.0c	145	3	3	1
T21101		✓	45		✓	0.25	2.0c	35	3	1	2
T22101		✓	45		✓	0.25	2.0c	145	3	1	2
T31101		✓	45		✓	0.25	2.0c	35	3	1	3
T32101		✓	45		✓	0.25	2.0c	145	3	1	3
U03501		✓	45		✓	0.25	2.0c	35	1	-	0
U03601		✓	45		✓	0.25	2.0c	35	2	-	0
U03701		✓	45		✓	0.25	2.0c	35	3	-	0
U14501		✓	45		✓	0.25	2.0c	145	1	-	0
U14601		✓	45		✓	0.25	2.0c	145	2	-	0
U14701		✓	45		✓	0.25	2.0c	145	3	-	0
V03501		✓	45		✓	0.25	2.0c	35	1	-	1
V03601		✓	45		✓	0.25	2.0c	35	2	-	1
V03701		✓	45		✓	0.25	2.0c	35	3	-	1
V14501		✓	45		✓	0.25	2.0c	145	1	-	1
V14601		✓	45		✓	0.25	2.0c	145	2	-	1
V14701		✓	45		✓	0.25	2.0c	145	3	-	1
W03501		✓	0		✓ (edge)	0.25	2.0c	35	1	-	0 (1:12)
W03601		✓	0		✓ (edge)	0.25	2.0c	35	2	-	0 (1:12)
W03701		✓	0		✓ (edge)	0.25	2.0c	35	5	-	0 (1:12)
W14501		✓	0		✓ (edge)	0.25	2.0c	145	1	-	0 (1:12)
W14601		✓	0		✓ (edge)	0.25	2.0c	145	2	-	0 (1:12)
W14701		✓	0		✓ (edge)	0.25	2.0c	145	5	-	0 (1:12)
X03501		✓	0		✓ (edge)	0.25	2.0c	35	1	1	0 (1:12)
X03601		✓	0		✓ (edge)	0.25	2.0c	35	2	1	0 (1:12)
X14501		✓	0		✓ (edge)	0.25	2.0c	145	1	1	0 (1:12)
X14601		✓	0		✓ (edge)	0.25	2.0c	145	2	1	0 (1:12)
Z03501	✓		0	✓		0.25	-	35	-	-	0 (1:12)